A STUDY OF THE DECAY MODES OF THE ^{9}Li NUCLEUS

Thesis by

Yu-Ssu Chen

In Partial Fulfillment of the Requirements

For the Degree of

Doctor of Philosophy

California Institute of Technology

Pasadena, California

1970

(Submitted September 15, 1969)

ACKNOWLEDGMENTS

I would like to thank the entire staff of the Kellogg Radiation Laboratory for the assistance and encouragement provided during the course of this work.

I am especially grateful to Dr. T. A. Tombrello for suggesting the problem and for his guidance during this investigation. I also like to express my gratitude to Dr. R. W. Kavanagh for his supervision during the course of the neutron-beta coincidence experiment. I am indebted as well to Dr. K. Nagatani for his participation in the early phase of the recoil-particle experiment.

I wish also to acknowledge the California Institute of Technology and Gulf General Atomic, Inc. for financial support.

Finally I wish to thank my wife, Mary, for her understanding and encouragement during the course of this work and for her help in drafting this thesis.

This research project has been supported in part by the National Science Foundation (GP - 9114) and the Office of Naval Research (Nonr - 220(47)).

ABSTRACT

The beta decay of the ^{9}Li nucleus and the subsequent particle decays of the unbound states of the ^{9}Be nucleus have been investigated with two complementary techniques – The recoil-particle method and the beta-neutron coincidence method. ^{9}Li nuclei were produced by the $^{18}O(^{7}Li, ^{9}Li)^{16}O$ reaction with a 20 MeV bombarding energy and by the $t(^{7}Li, ^{9}Li)p$ reaction with a 14 MeV bombarding energy. The energy spectrum of the delayed alphas and the time-of-flight spectrum of the delayed neutrons were obtained. The half life was also measured and was found to be 177 ± 3 msec. Besides the known decay branches to the ground state and to the 2.43 MeV state in ^{9}Be, a new decay branch to an unbound state in ^{9}Be at an excitation energy of 2.78 ± 0.125 MeV was observed. The branching ratios and the log ft values were found to be;

$(65.0^{+2.7}_{-2.4})\%$, $(32.0^{+2.7}_{-3.7})\%$, $(3.0^{+2.7}_{-0.3})\%$ and

$(5.12^{+0.01}_{-0.02})$, $(5.00^{+0.04}_{-0.05})$, $(5.97^{+0.05}_{-0.28})$ to the ground state, the 2.43 MeV and the 2.78 MeV states, respectively. The observed properties of the 2.78 MeV state favor an assignment of $1/2^{-}$. It decays mainly by p-wave neutron emission to the ground state of ^{8}Be and has center-of-mass width of 1.1 ± 0.125 MeV.

The fraction of the decays of the 2.43 MeV state in ^{9}Be involving emission of an f-wave neutron to the ground state of ^{8}Be was found to be $(6.4 \pm 1.2)\%$.

TABLE OF CONTENTS

PART	TITLE	PAGE
I	INTRODUCTION	1
II	EXPERIMENTAL METHODS	5
	A) The Recoil-Particle Method	5
	1) The ^{7}Li Beam and the Target Preparation	5
	2) Detectors	6
	3) Particle Identification System	7
	4) Experimental Procedure	8
	5) Calibrations	10
	6) Background Determination	11
	B) Beta-Neutron Coincidence Method	11
	1) Target Assembly	12
	2) Detectors and Electronics	12
	3) Experimental Procedure	14
	4) Calibrations	15
	5) Efficiency of the Neutron Counter	17
	C) Half Life Measurement	18
III	EXPERIMENTAL RESULTS	19
	A) Half Life of the ^{9}Li Nucleus	19
	B) Delayed Neutron Spectrum	19
	1) The Newly Observed 2. 78 MeV State in ^{9}Be	20
	2) Branching Ratios and their Errors	26
	C) Delayed Alpha Spectrum	27
	1) The Ground State Branch of the ^{9}Li Decay	28
	2) Comparison with the Neutron Spectrum	30
	3) Decay Modes of ^{9}Li and Branching Ratios	31

PART	TITLE	PAGE
IV	DISCUSSION	32
	A) Rotational Model Interpretation	32
	B) Intermediate Coupling Shell Model Interpretation	40
	C) Conclusions	43
APPENDIX I	Determination of the Bias of the Neutron Detector	44
APPENDIX II	Nilsson Model Calculation	46
APPENDIX III	Calculation of the ft Value and the Reduced Width	49
REFERENCES		52
TABLE		54
FIGURES		56

I. INTRODUCTION

Various nuclear models have been applied to study the lp shell nuclei during past years. This is primarily due to the simplicity of the configurations. By assuming the lowest $(ls)^4(lp)^{A-4}$ configuration, several intermediate coupling shell model calculations have been made for the normal parity states in these nuclei (see, for example, Kurath 1956). Most recently, Cohen and Kurath (1965) have carried out a complete study on the lp shell nuclei by parametrizing the matrix elements for the two body interaction and two of the single particle energies. Parameters in the theories are usually obtained by fitting the positions of the energy levels. The resultant wave functions were used to calculate various quantities, such as the magnetic dipole moments, the M1 transition matrix, the Gamow-Teller beta decay matrix, etc. In general, the results are in good agreement with experimental data. A remarkable feature of the models is the ability to match up the predicted low lying states with the experimental observations. The lack of one to one correspondence is extremely rare; nevertheless, such exceptions do exist and have not yet been resolved. One of the disturbing examples is in the ^{9}Be nucleus. The energy level diagram of the ^{9}Be nucleus is shown in figure 1, which is taken from Lauritsen and Ajzenberg-Selove (1966).

In the L-S coupling limit, which is a good approximation for the very light nuclei, the low lying states of ^{9}Be are composed of degenerate ^{22}P, ^{22}D and ^{22}F states. They should further be split into two bands under the spin-orbit residual interaction. The lower band with states of J^π equal to $3/2^-$, $5/2^-$ and $7/2^-$ has been identified as the ground state, the 2.43 MeV and the 6.76 MeV states.

The spin and parity assignments are based on the following experimental results. From the magnetic resonance absorption data by Schuster and Pake (1951), the J^{π} of the ground state is known to be $3/2^-$. The $5/2^-$ assignment for the 2.43 MeV state is a result of direct reaction interpretations of inelastic proton, deuteron and alpha scattering angular distributions given by Summers-Gill (1958) and by Schrank, et al. (1962). It is also obtained by Barber (1960) and by Edge and Peterson (1962) from the predominant M1 excitation of the inelastic electron scattering at large angles. Furthermore, the strong collective excitation of the 2.43 MeV and 6.76 MeV states in the inelastic proton scattering suggested that they are members of a rotational band. The 6.76 MeV state should have $J^{\pi} = 7/2^-$. Indeed, Ngoc (1963) showed that it is also strongly populated in the inelastic electron scattering by E2 excitation from the ground state. The neutron widths of excited states in ^{9}Be has been extensively studied by Christensen and Cocke (1966). A result, which is used as a check on the accuracy of the present experiment, is the observed f-wave decay of the 2.43 MeV state. It can only arise from the major shell mixing of the wave function. A successful explanation based on the rotational model was given by Stephenson (1966). Although the lower band has been positively identified, the higher band ($1/2^-$, $3/2^-$, $5/2^-$) has not yet been observed directly. Assuming a reasonable spin-orbit interaction strength, the lowest member of the higher band, namely, a $J^{\pi} = 1/2^-$ state, is predicted by various authors at 2 to 3 MeV in excitation energy (see, for example, Barker (1966) and Bouten, et al. (1969)). Since the emission of a p-wave neutron to the ground state of ^{8}Be is allowed, a large neutron width is expected for this state. Moreover, the effort to locate such a state using a nuclear reaction is further

shadowed by the existence of two broad non-normal parity states situated at excitation energies of 1.67 MeV ($1/2^+$, Γ = 200 keV) and 3.03 MeV ($5/2^+$, Γ = 300 keV). Nevertheless, indirect evidence for the existence of a $1/2^-$ state in this energy region is furnished by the asymmetrical shape of the 3 MeV resonance in the ^{9}Be(γ, n) total cross-section by Phillips (1968) and by the ^{9}Be(e, e') data of Clerc (1968).

Recently, Chen, et al. (1968) have pointed out that the negative parity states in ^{9}Be should be preferentially populated by the allowed Gamow-Teller beta decay of ^{9}Li, which has a $3/2^-$ ground state. Therefore, a detailed study on the ^{9}Li decay may turn out to be fruitful in locating the 'missing' $1/2^-$ state.

The ^{9}Li activity has been known since 1951. The half life has been measured by several authors and the mean value is summarized in Lauritsen and Ajzenberg-Selove (1966) as 172 ± 3 msec. It is also known as a delayed neutron emitter, since there are branches to unbound states of ^{9}Be. A previous study on the decay modes of ^{9}Li was made by Alburger (1963). The ^{9}Li nuclei were produced by irradiating a ^{9}Be sample with neutrons from the t + d reaction. Both the beta spectrum and the β - n coincidence spectrum from the ^{9}Be sample were taken. Two end-point energies from the decays were observed. A shape analysis on the beta singles spectrum indicated that (25 ± 15)% of the decays are to the ground state and (75 ± 15)% to the 2.43 MeV state. The corresponding log ft values were (5.5 ± 0.2) and (4.7 ± 0.2), which support the assumption of an allowed Gamow-Teller beta decay and a $J^\pi = 3/2^-$ assignment for the ^{9}Li nucleus. A different branching ratio, however, was obtained by Nefkens (1963), who had observed all the beta activities induced by 320 MeV bremsstrahlung in a boron target. A ^{9}Li component

was established. Together with a previous measured cross-section on the delayed neutrons from the $^{11}B(\gamma, 2p)^{9}Li$ reaction by Tautfest (1958), the ground state decay branch was found to be 50-70%. During the course of the present work, the delayed neutron spectrum following the beta-decay of ^{9}Li was studied by Macefield, et al. (1969) using a time-of-flight spectrometer. In addition to the previous established decay branches, a neutron group corresponding to a new decay branch to a state at an excitation energy of 3.0 ± 0.1 MeV in ^{9}Be was clearly seen. However, high background counts in the time-of-flight spectrum make the extracted branching ratio rather doubtful.

In part II of this thesis, the experimental details used to investigate the decay modes of ^{9}Li are described. The results of the measurements are given in part III. Finally, in part IV, a discussion of the results is presented.

II. EXPERIMENTAL METHODS

The beta decay of the ^{9}Li nucleus and the subsequent particle decays of the excited states of the ^{9}Be nucleus have been investigated with two complementary methods: the recoil-particle method and the neutron-beta coincidence method. The energy spectra of the delayed charged-particles and neutrons emitted from excited states of ^{9}Be have been obtained. Experimental details are given in sections A and B, respectively. In section C, a half life measurement on the ^{9}Li nucleus will also be discussed briefly.

A. The Recoil-Particle Method

A $Ni^{18}O$ target was bombarded with a 20 MeV $^{7}Li^{+++}$ beam. The $^{9}Li^{+++}$ ions from the reaction $^{18}O(^{7}Li, ^{9}Li)^{16}O$ were analyzed at 10^{o} with a 61 cm double-focusing magnetic spectrometer and identified with a $\Delta E \times E$ counter telescope positioned at the focal point of the spectrometer. The ^{9}Li nuclei decayed inside the rear detector, allowing the delayed alpha spectrum to be measured.

1) The ^{7}Li Beam and the Target Preparation

The ^{7}Li beam was obtained from the CIT-ONR tandem accelerator. Negative ^{7}Li ions were extracted from a modified HVEC negative ion source. The exchange canal inside the ion source box was replaced by a lithium boiler filled with natural lithium metal (93% ^{7}Li). A heating coil with a reflector permitted the vaporization of the lithium, and the vapor was bombarded with an intense proton beam. Approximately 0.5 μA of Li^{-} ions could be extracted

from the boiler for continuous periods of up to two days. The average beam intensity on the target during the runs was about 100 nano Amperes.

The $Ni^{18}O$ target was made by heating a 2500 $\mathring{A}$ nickel foil in an oxygen atmosphere enriched in ^{18}O. It contains approximately 0.23×10^{19} ^{18}O atoms per cm^2.

2) Detectors

At the focal point of the spectrometer a set of $\Delta E \times E$ solid state detectors was used to measure the energy loss as well as the total energy of the recoiling particle. Although the $^9Li^{+++}$ ions have energy of 13.6 MeV, they have a rather short range, approximately 41 microns, in the silicon detector. Therefore, a 26-micron transmission silicon detector was chosen as the ΔE detector. The choice of the E detector is based on compromising two conflicting requirements. The E detector was not only used to detect ^9Li ions, but also was used to measure the energy deposited by all charged particles following the beta decay during the beam-off cycle. Because of the many-particle nature of the decay, the total energy of the charged particles (predominately due to the delayed alphas) can be as low as 90 keV. The noise level of a typical thin silicon detector out of a low noise preamplifier is about 50 keV, which is comparable to the signal level. A way to reduce the noise is to decrease the detector capacitance by increasing its thickness. Therefore, in principle, a thicker detector is preferable from this consideration. However, there exists a decay branch in which the ^9Li nucleus decays to the ground state of the ^9Be, which is particle stable. The only energy

deposited in the E detector following the decay is, in this case, due to the high energy beta particle which loses about 0.5 keV per micron in the silicon detector. If one wishes in analyzing the spectrum to distinguish these events from those which do give rise to delayed alpha particles, a very thin E detector is needed to reduce the beta pulse height. A 29-micron thick, 50 mm^2 area transmission silicon detector was finally chosen as the E detector. The average energy loss for the beta particles in this detector is thus kept less than 100 keV. The noise level of the system was further reduced by cooling the detectors. This was accomplished by mounting the detectors on a copper rod kept at dry ice temperature. Surrounding the detectors was a cylindrical brass shield in thermal contact with a liquid nitrogen trap. The arrangement was necessary to prevent of build-up of a thin dead layer on the cold surfaces of the detectors. The whole detector assembly is shown in figure 2.

3) Particle Identification System

A particle identification system based on the analyzing power of the magnetic spectrometer and the dependence of the energy loss of a particle on its mass and charge was used to separate various recoiling particles. The electronic block diagram is shown in figure 3. Tennelec model 100A low noise preamplifiers were used for both detectors. The ΔE and E signals from the preamplifiers were sent separately through an Ortec model 410 or a RIDL model 30-23 linear amplifier and then to Ortec model 400 timing single channel analyzers. The summed signal from a coincidence mixer, balanced for both the ΔE and E input channels with proper attenuations of the outputs from the preamplifiers, was also sent

through an Ortec model 410 linear amplifier and Ortec model 400 single channel analyzer. The logic signals from all the single channel analyzers were required in slow coincidence by two parallel Ortec model 409 linear gate and slow coincidence units. The outputs from the linear amplifiers of ΔE and $E + \Delta E$ channels after being delayed for 1.2 μsec were used separately as the inputs for the two linear gate and slow coincidence units.

For a given magnetic field of the spectrometer, the particle detected at the focal point should have energy proportional to the Z^2/M, where Z is the charge and M is the mass of the particle. Furthermore, the energy losses for various charged particles in the ΔE detector for a given magnetic field of the spectrometer should be proportional to M^2. Therefore, with properly adjusted windows on the $E + \Delta E$ and ΔE single channel analyzers, one can pick out a specific kind of ion. In particular, $^9Li^{+++}$ (or $^8Li^{+++}$) ions were picked out by this method in the present experiment. The coincidence requirement on the E channel was simply to eliminate all heavier ions, which had been stopped in the ΔE detector. The coincidence output from one of the linear gates was then used to gate a sequence timer, which initiated a counting cycle for the delayed charged particles.

4) Experimental Procedure

Once a $^9Li^{+++}$ ion (or $^8Li^{+++}$ ion) was identified by the system described above, a gating pulse was sent to a sequence timer and to a scaler which recorded the total number of ^9Li (or ^8Li) nuclei produced. Various logic signals generated by the sequence

timer were used to execute the following steps, which are shown schematically in figure 4.

a) The beam was deflected away from target for a total period of T_1 msec.

b) Following a short waiting period of T_2 msec after the beam was turned off, the analyzer was unblocked for two successive periods of T_3 msec. T_3 was chosen approximately to be the mean life of ^{9}Li nucleus (or ^{8}Li nucleus). During these periods the $^{9}Li^{+++}$ ion (or $^{8}Li^{+++}$ ion) can decay in the E detector, giving rise to a pulse whose amplitude is proportional to the total energy deposited in it from all the delayed charged particles. The pulse is amplified and sent to a RIDL 400 channel analyzer. Events from the two successive periods were analyzed and stored in their respective 200 channels sections of the memory.

c) After the completion of a counting cycle, the beam was turned back on and the analyzer was blocked again.

Such a cycle repeated itself whenever a $^{9}Li^{+++}$ ion (or a $^{8}Li^{+++}$ ion) was produced. Because of the extremely low production yield of ^{9}Li ions as given by Nettles (1969), this procedure has proven to be more efficient than the usual method to study activities, namely, where each cycle has fixed portions of beam on and off time.

In this manner, a delayed charged particle spectrum corresponding to a given number of parent nuclei was obtained.

5) Calibrations

The entire system described in the previous sections was checked and calibrated for $^{8}Li^{+++}$ ions which were produced along with $^{9}Li^{+++}$ ions in the present reaction. The recoiling ^{8}Li ions entered the spectrometer at an energy of 13.65 MeV, which is sufficient to allow them to get through the ΔE detector. The decay mode of ^{8}Li nucleus is well known. The beta decay with a half life of 850 msec leads mainly to the 2.9 MeV state of ^{8}Be, which is particle unstable and breaks up into two alpha particles. Two delayed alpha spectra were taken with T_3, T_2 adjusted to 850 msec, 20 msec (see section 4) and with the spectrometer and the windows on the $\Delta E + E$ and ΔE channels set for $^{8}Li^{+++}$ ions. They correspond separately to the periods of the first and second half lives after the beta decay of a ^{8}Li nucleus. The ratio of the yields between the first and second halves was found to be 2.12 ± 0.15. Within statistics, that is what one expected. The sum of these two spectra is shown in figure 5. The spectrum shapes agree quite well with the result obtained by Alburger, et al. (1963). The broad peak at 3 MeV is due to the break up of the 2.9 MeV state of ^{8}Be into two alpha particles. The change in the slope around 5 MeV is a direct indication that the ^{8}Li ions were buried in the E detector at a depth of approximately 19 microns. As a result, if the total energy for the two delayed alpha particles exceeds 5 MeV, one of them might not lose all its energy in the E detector. This leads to the enhancement in the yield at about 5 MeV. Evidently the range of 13.6 MeV $^{8}Li^{+++}$ ions in silicon is approximately 45 microns. Using this experimental value, the corresponding range of 13.6 MeV $^{9}Li^{+++}$ ions was estimated to

be 41 microns. The recoiling $^{9}Li^{+++}$ ions having this energy will thus come to rest inside the E detector at a depth of 15 microns. Fortunately, it is sufficient to stop all the low energy delayed alpha particles following the ^{9}Li decays. The peak position in the delayed alpha spectrum of ^{8}Li also provided an excellent energy calibration point for the E detector.

6) Background Determination

The only background in the spectrum was the rather low level electronic noise associated with the E detector during the counting cycles. With the beam stopped outside the target room, pulses from a 60-cycle pulser were used to generate equivalent gating pulses. A separated background run was then taken in the same manner described in section 4. The total number of gates in this case was chosen to be the same as for the delayed charged particle spectrum. Nearly all the background counts were found to be below 80 keV.

B) Beta-Neutron Coincidence Method

Previous experiments that have examined the delayed neutrons by Alburger (1963) and Tautfest (1958) have not been well adapted for an accurate measurement of their spectrum. In the present method, the ^{9}Li nuclei were produced by bombarding a ZrT target with a 14 MeV $^{7}Li^{+++}$ beam. The associated particle (in this case, an electron from the beta decay of ^{9}Li nucleus) time-of-flight technique was used to provide the necessary energy resolution for the neutrons. A similar experiment has recently been performed by Macefield (1969) using the $^{7}Li(t, p)^{9}Li$ reaction. The background there, mainly from

the ^{8}Li and ^{6}He activities associated with the tritium beam posed a serious problem. However, by reversing the roles of the projectile and the target a considerably cleaner delayed neutron spectrum was obtained. The bombarding energy chosen was below the threshold for ^{8}Li production by $t(^{7}Li, ^{8}Li)d$.

1) Target Assembly

A ZrT target (made by the Isotopes Division of the Oak Ridge National Laboratory) was used. The Zr was evaporated on a 1" diameter, 10 mil thick platium backing and is approximately 1500 $\mu g/cm^2$. The target was held between two 30 mil thick tantalum discs. Both discs had a 1/2" hole at the center which defined the target area. The holder with the target was then held by a 1/16" thick aluminum plate against the end of a beam tube cut at a 45 degree angle. The total amount of tritium on target is about 4 Curies, which is equivalent to 10^{19} tritium atoms/cm^2. No target cooling was needed for the average 100 nano-Ampere ^{7}Li beam. The beam spot was made approximately 3/8" in diameter. A liquid nitrogen cooled absorption trap placed 8" in front of the target prevents organic vapors from reaching the target.

2) Detectors and Electronics

The beta counter is a 2" x 0.6" Pilot-B crystal mounted on an RCA 8575 photo-multiplier tube. It was enclosed inside an aluminum can with a 3/16" thick aluminum end piece in front of the crystal and was positioned at 45^{o} with respect to the beam axis right against the target assembly. A total of 1/4" of aluminum was between the

target and the beta counter. The purpose of the aluminum was to attenuate low energy beta particles produced by nuclei other than ^{9}Li, specifically the ^{6}He's. Using the empirical formula for the electron ranges in the aluminum given by Katz and Penford (1952), the energy loss of beta particles in aluminum was found to be 3.2 MeV. Since the end point energy of the beta spectrum from the ^{9}Li decay is above 11 MeV, a large portion of the spectrum was still preserved. 2000 volts was applied to the anode of the photomultiplier. The anode signal from the beta counter was delayed with a 77-ft RG58 cable (equivalent to 120 nsec) and was used as the input to the stop side of an Ortec model 437 time-to-pulse height converter (TAC). The positive linear signal from the 10th dynode of the RCA 8575 was amplified and analyzed by an Ortec model 400 timing single channel analyzer. A lower level discriminator was then set in the single channel analyzer to cut off all γ-ray pulses below 1.2 MeV. The energy scale of the linear signal was established by calibrating against the Compton edges of a ^{60}Co and a ^{137}Cs source. Together with the 1/4" aluminum absorber, a total of 4.44 MeV bias was introduced in the beta channel. The output of the single channel analyzer was then fed to a scaler, which monitored the counting rate of the beta counter, and to the delayed coincidence input of a RIDL 400 channel pulse height analyzer. Therefore, with the delayed coincidence gate on, only those TAC signals corresponding to beta gate pulses greater than 4.44 MeV were analyzed.

A 5" $\times$ 2" Pilot-B crystal with an Amperex XP1040 fast photomultiplier tube was used as the neutron counter, which was placed at 90^{o}, 28 cm away from the target on the opposite side from the beta counter. 2250 volts was applied to the anode of the phototube. Anode pulses having a rise time of approximately 3 nsec were

used to start the TAC. Since the excited states of ^{9}Be can break up into three particles (two alphas and a neutron), the emitted neutrons can have energies ranging from zero up to eight-ninths of the total break-up energy. In principle, one would like to be able to detect very low energy neutrons as well as energetic neutrons. Therefore, no explicit bias was introduced in the neutron channel, except that from the fixed internal discriminator in the TAC. The neutron energy bias corresponding to this discriminator setting was determined to be 80 keV. Details are given in appendix I. The linear signal from the photo-tube was amplified and fed into a scaler, which only served as a monitor for the neutron counter.

The output from the TAC was analyzed by a RIDL 400 channel analyzer. During the initial set up stage, a ^{22}Na source was placed close to the target position. The two .511 MeV annihilation γ-rays and the .511 MeV and 1.28 MeV coincidence γ-rays provided sources to allow various delays and gains to be set properly. The electronic block diagram is shown in figure 6.

3) Experimental Procedure

The experimental procedure was similar to the one discussed in the Recoil-Particle method with the exception that the sequence timer was ungated and was operating in a continuous mode. As in the recoil experiment, T_3 was chosen to be the mean half life of ^{9}Li nucleus. A relay switch driven by the "beam-on" pulse controlled the beam deflecting magnet. The "beam-on" pulse plus the waiting pulse were used to block the RIDL analyzer. The beam-on time (T_0) was set to be 310 msec.

4) Calibrations

The absolute time scale for the neutron time-of-flight spectrum was obtained in the following manner. The coincidence γ-γ peak from the ^{22}Na source was used as the zero time reference. Three RG58 cables of different lengths and their various combinations were inserted into the neutron side (start side) of the TAC. The actual cable length for each configuration was carefully measured by sending sinuosidal waves down the line (shorted at the opposite end) and recording the frequencies for the standing wave minima. Results of the cable calibration are shown in figure 7. The positions of the γ-γ peak in the time-of-flight spectrum was plotted versus the cable lengths. The absolute time scale was found to be 0.641 nsec/channel. Moreover, all the calibration points with the exception of one in channel 25 lie on a straight line, which is a positive indication that the TAC is essentially linear above channel 30. Another independent check on the linearity was also performed. A ^{22}Na source was placed at the target position and a ^{137}Cs source was placed in front of the neutron counter. With 6" lead bricks separating these two sources, a random time spectrum was taken. The result is shown in figure 8. Within statistics, it shows a complete flat spectrum above channel 30. The peak in channel 151, of course, is understood to be the coincident γ-rays from the ^{22}Na source scattered into the counters. Below channel 30, however, a large non-linearity is observed. Fortunately, with the flight path of 28 cm and the γ-γ peak in channel 151, the region below channel 30 corresponds to neutrons having energies below 90 keV, which is in the neighborhood of the neutron bias. The relative efficiency of the neutron counter in this energy range is not well defined. As a

result, this portion of the spectrum has always been discarded. The overall time resolution, obtained by examining the γ-γ coincidence peak in the spectrum, was found to be less than 2 nano-seconds.

Although the time scale was shown to be linear, the neutron energy E_n, is by no means simply related to the flight time t with the ideal equation. That is

$$E_n = m_n c^2 \left(\frac{1}{\sqrt{1 - \left(\frac{L}{tc}\right)^2}} - 1 \right)$$

where m_n is the neutron rest mass, L is the flight path and c is the velocity of light. The deviation from this equation arises mainly for the following reason. The start side of the TAC is always triggered at a time when the input neutron pulse rises above a fixed voltage V_o. Therefore, for two neutron pulses with different pulse heights, or, in other words, with two different rising slopes, a net time difference has already been introduced. This time difference could be as large as the rise time of the pulses, which is about 3 nano-seconds. A detailed experimental investigation of the neutron energy versus its flight time was obviously needed. A ^{14}C target was placed in the target holder and was bombarded with 3.4, 3.5, 3.6, 3.8, 4.0, 4.5 and 5.0 MeV protons. The flight time of the mono-energetic neutrons emitted from the reaction $^{14}C(p,n)^{14}N^*$ was measured with the same experimental set up. The 2.31 MeV or the 3.95 MeV γ-rays emitted from the first and second excited states of ^{14}N were used to stop the TAC. The results are shown in figure 9. The solid curve is a one parameter least square fit to the data points. The

analytic expression of E_n as a function of t used there is

$$E_n = m_n c^2 \left(\frac{1}{\sqrt{1 - \left(\frac{L}{\tau \cdot c \cdot \Delta C} \right)^{\theta}}} - 1 \right)$$

with θ as a free parameter, where ΔC is the channel difference between the γ-γ peak and the neutron peak. τ is the time scale (0.641 nsec/channel). The value of θ, which produced the best fit, was found to be 1.934 ± 0.019. Not surprisingly, it is not equal to 2; nevertheless, it is close to the exact value. From the quality of the fit, it is reasonable to conclude that such a simple expression is quite adequate to represent the actual experimental situation.

5) Efficiency of the Neutron Counter

The relative efficiency of the 5" x 2" Pilot-B crystal with the present 80 keV bias was measured in the following way. The neutron yields at 0° from the $^{7}Li(p,n)^{7}Be$ reaction for various proton bombarding energies were compared with an earlier measurement by Taschek (1948). A pulsed proton beam from the CIT-ONR tandem Van de Graaff was used in this case to provide the stop signal for the TAC. The measured result of the relative efficiency is shown in figure 10. A smooth curve is drawn through the data points, and is later used for correcting the raw delayed neutron spectrum. Except for neutrons having energies below 200 keV, the relative efficiency curve is believed to be accurate within $\pm 10\%$. No absolute efficiency measurement has been made, since it is irrelevant to the present problem.

C) Half Life Measurement

In this series of experiments, the ^{9}Li half life was also measured by detecting the beta activity. The ^{9}Li nuclei were produced by the same reaction, $t(^{7}Li, ^{9}Li)p$, with a 14 MeV bombarding energy. The beta counter and its geometrical configuration were the same as described in section B. A total of 5/16" of aluminum plates was placed between the ZrT target and the beta crystal. A positive 1100 volts was applied to the photo anode. The anode signals were amplified by a Tennelec TC200 linear amplifier. A beta bias set to cut off the Compton edge of ^{60}Co was introduced by the TC250 biased amplifier and stretcher. The negative 5 volt strobe out pulse was then used as the data input to the RIDL 400 channel analyzer, operating in a time sequence mode (TSS). The time base was determined by an external oscillator unit, RIDL model 56. It has two crystal controlled oscillators which are accurate to $\pm 0.1\%$. The electronic block diagram is shown in figure 11. Again the sequence timer operating in a continuous mode controlled the experimental cycles. Each cycle begins with a 350 msec beam-on period. The external oscillator upon receiving the beam-on pulse from the sequence timer started its oscillation and caused the RIDL analyzer to operate accordingly. After the 350 msec beam-on period, the beam was deflected away from the target and stayed off until the completion of the full 400 channels. The address overflow command from the RIDL analyzer was used to stop the external oscillator. The entire time sequence is best illustrated in figure 11. Data were taken for both 5 msec/channel and 20 msec/channel time bases. Long half-life background activities up to the order of a few seconds were thus included in the spectrum.

III. EXPERIMENTAL RESULTS

A) Half Life of the ^{9}Li Nucleus

The beta activities from the bombardment of the ZrT target with 14 MeV $^{7}Li^{+++}$ beam are shown in figure 12. The solid line represents the result of a three-parameter non-linear least square fit with three decaying components. The weaker components with 4% and 8% of the total yield were assumed to be from ^{8}Li and ^{16}N, which have half lives of 850 msec and 7.4 sec respectively and are high energy beta emitters. They can be produced from the target contaminants — deuterium, carbon, etc. The half life of ^{9}Li (the prominant component) is found to be 177 ± 3 msec, which is in agreement with the mean value given by Lauritsen and Ajzenberg-Selove (1966). The quoted error does not represent the result of the particular fit, but rather indicates the range of the ^{9}Li half life obtained from various two parameter fits. The value of 177 ± 3 msec is later used to calculate the log ft values for all the beta decay branches of the ^{9}Li nucleus.

B) Delayed Neutron Spectrum

A time-of-flight spectrum with the flight path of 28 cm for the delayed neutrons was obtained with a total of 1800 μcoulombs $^{7}Li^{+++}$ bombardment on the ZrT target. The spectral shapes, which are shown in figure 13, of the first half and the second half are practically identical. The flat random coincidence backgrounds above channel 160 were extrapolated back into lower channels and later subtracted. Also subtracted was the peak around channel 148, which

is essentially due to the bremsstrahlung-β real coincidences. The ratio of the neutron yields between the first and second halves was found to be 2.4. It should compare with the ideal value

$$e^{T_3/\tau} = 2.65 \pm 0.3 ,$$

where T_3 is the counting period, (250 ± 10) msec, and τ is the mean life of ^{9}Li, (247 ± 4) msec. The sum of the two resultant spectra with the correction of the relative neutron efficiency (see part II, section 5) is shown in figure 14. The absolute neutron energy scale is obtained from the $^{14}C(p, n\gamma)^{14}N$ calibration (see part II, section 4).

Three neutron groups situated approximately at neutron energies of 0.3, 0.65 and 0.95 MeV are clearly seen. The broad peak at 0.3 MeV (denoted by P1 in figure 14) is due to the break up of the 2.43 MeV state of ^{9}Be into a neutron and two alpha particles. The narrow peak at 0.65 MeV (P2) is due to the break up of the same state into a neutron and the ground state of ^{8}Be, which breaks up into two alphas. The peak at 0.95 MeV (P3) is attributed to a new state in ^{9}Be, which breaks up almost entirely into a neutron and the ground state of ^{8}Be. The assignment of these peaks will become clear as more evidence is presented below.

1) The Newly Observed 2.78 MeV State in ^{9}Be

The separation of these three peaks relies, first of all, upon a reasonably good theoretical fit to the broad peak P1, since a considerable amount of the high energy tail of P1 extends into

P2 region. Under the assumption that the break up mechanism for the 2.43 MeV state is sequential, that is

$$^{9}\mathrm{Be}\ (2.43) \rightarrow {}^{8}\mathrm{Be} + \mathrm{n}, \quad {}^{8}\mathrm{Be} \rightarrow \alpha + \alpha \ ,$$

the neutron yield in the laboratory was calculated. The equation used is given by Cocke (1967):

$$\frac{dY(T_n)}{dT_n} = \text{const.}\ (k_n R_n P_{\ell_n}(k_n R_n))_{^{8}\mathrm{Be}+\mathrm{n}} \left(\frac{\sin^2 \beta_\ell}{kRP_\ell(kR)}\right)_{\alpha+\alpha} .$$

The first term includes the centrifugal barrier penetration factor and the phase space factor for the neutrons. The second term represents the enhancement of the yield due to the final state interaction between the two alphas. The symbols in the equation are:

T_n = neutron laboratory energy

k_n = wave number for the ^{8}Be + n system

R_n = channel radius for the ^{8}Be + n system

ℓ_n = ℓ_nth partial wave between ^{8}Be and neutron

ℓ = ℓ-th partial wave for α-α scattering

k = wave number for the $\alpha + \alpha$ system

R = channel radius for the $\alpha + \alpha$ system

$P_\ell(kR) = \dfrac{1}{F_\ell^2(kR) + G_\ell^2(kR)}$, where F_ℓ and G_ℓ are the regular and irregular Coulomb (or neutron) wave functions.

$\beta_\ell = \delta_\ell + \varphi_\ell(kR)$

δ_ℓ = ℓ-th wave nuclear phase shift for α - α scattering.

The solid curve in figure 15 shows the incoherent sum of two such calculations including both s- and d- waves contributions from the α - α scattering. The parameters used are consistent with $J^\pi = 5/2^-$ for the 2.43 MeV state.

$\alpha + \alpha$ channel:

$R = 4.0$ fm

$\ell = 0$ or 2.

The nuclear phase shifts δ_0 and δ_2 are taken to be zero in the present energy range.

^{8}Be + n channel:

$R_n = 4.35$ fm

$\ell_n = 1$ or 3.

The same curve was also shown in the time-of-flight spectrum (see figure 14). The fit to the data points is normalized at the peak position. It is quite successful. The rise of data points below 100 keV is probably due to the rather large uncertainty of the relative efficiency near the 80 keV neutron bias. As mentioned before, since the decay modes of the excited states of ^{9}Be involve

three-particle final states, the neutrons can have energies from zero up to eight-ninths of the total break up energy. The neutron spectrum below the 80 keV bias is not readily available from the time-of-flight method. Hence, the calculated curve was used to estimate the neutron yield below the neutron bias.

The contribution from another possible break up mechanism,

$$^{9}\mathrm{Be}\ (2.43) \rightarrow {}^{5}\mathrm{He} + \alpha \qquad \llcorner\!\!\rightarrow\ n + \alpha\ ,$$

has also been investigated. The neutron yield was calculated with the following equation (see Cocke, 1967);

$$\frac{dY(T_n)}{dT_n} = \text{const.} \int_0^{E_o} \frac{1}{vw} \left(kRP_{\ell}(kR)\right)_{^{5}\mathrm{He}+\alpha} \left(\frac{\sin^2 \beta_{\ell'}}{k'R'P_{\ell'}(k'R')}\right)_{n+\alpha} dE_x$$

where

v = the recoil velocity of ^{5}He (assuming that the ^{9}Be* is at rest);

w = the neutron velocity with respect to the ^{5}He center of mass,

The factor 1/vw is the result of assuming that ^{5}He breaks up isotropically in its center-of-mass system.

E_o = The total energy available from the decay of ^9Be into $\alpha + \alpha + n$

E_x = The excitation energy of ^5He relative to the $\alpha + n$ threshold.

The rests of the notation is obvious. The parameters used are:

$^5He + \alpha$ channel

$R = 4.35$ fm

$\ell = 2$

$^4He + n$ channel

$R' = 3.00$ fm

$\ell' = 1$.

The $p_{3/2}$ phase shifts for the $^4He + n$ system is taken from the calculation by Tombrello (1966).

The result of such a calculation, however, failed to reproduce the spectral shape. It was concluded that the contribution from the $^5He + \alpha$ intermediate state to the neutron yield must be quite small (less than 20%).

Another particle decay branch of the 2.43 MeV state of ^9Be is through f-wave neutron emission to the ground state of ^8Be. It has been observed by several authors. The measured neutron width of the state is less than 1 keV. The emitted f-wave neutrons, in this case, should have a well defined energy E_n, which is given by

$$E_n = \frac{8}{9} \times (2.430 - 1.67)\ \text{MeV} = 0.676\ \text{MeV} \ .$$

The peak P2 after the removal of the broad peak P1 is situated at a neutron energy (0.655 ± 0.032) MeV. Therefore, from the energy consideration, the origin of this narrow peak is unambiguously determined. The observed width of approximately 300 keV (or 6.5 nsec) indicates the overall instrumental resolutions.

Under the assumption that P3 is the result of a p-wave neutron emission from a $J^{\pi} = 1/2^{-}$ (or a $3/2^{-}$) state in ^{9}Be nucleus to the ground state of ^{8}Be and with the inclusion of the weighting factor f(+Z, E) due to the preceeding beta decay, a single level R-matrix resonance formula (see Cocke, 1967)

$$\frac{kRP_{\ell}(kR)\,\theta^2}{(E - E_R)^2 + \Gamma^2/4}$$

with R = 4.35 fm and $\ell = 1$ has been used to fit the high energy portion of the spectrum. The result is shown in figure 16. The resonance energy and the width were determined to be

$$E_R = (1.00 \pm 0.1)\ \text{MeV}$$

$$\Gamma = (0.98 \pm 0.1)\ \text{MeV},$$

or, in terms of the excitation energy in ^{9}Be, it corresponds to a state in ^{9}Be at an excitation energy of (2.78 ± 0.125) MeV with a neutron center-of-mass width of (1.1 ± 0.125) MeV. The results are consistent with the data of Macefield (1969). The reduced width in units of $\hbar^2/MR^2$ (= 2.47 MeV) is found to be 0.48 ± 0.06.

The relative neutron yields for the three peaks are summarized as the following:

P1 : P2 : P3 = 14.72 : 1.00 : 1.45

2) Branching Ratios and their Errors

The neutron decay of the 2.43 MeV state of ^{9}Be to the ground state of ^{8}Be has been studied in considerable detail by Christensen and Cocke (1966). The branching ratio was found to be (7.5 ± 1.5)%. Since the beta decay of ^{9}Li nucleus also populated this $5/2^{-}$ state (see previous section), naturally, the known branching ratio should be used as an internal check for the present experimental set up. From the relative neutron yields between P1 and P2, the branching ratio is found to be (6.4 ± 1.2)%. It is in excellent agreement with the Christensen and Cocke measurement. The quoted error includes:

a) uncertainty due to the extrapolation of the spectrum toward zero neutron energy, (±5%);

b) separation of the peaks, (±15%);

c) uncertainty due to the relative efficiency of the neutron counter, (±10%).

Another important branching ratio, which can be deduced from the spectrum is the relative population of the 2.43 MeV state and the newly observed 2.78 MeV state in ^{9}Be from the ^{9}Li beta decay. However, attention must be paid to the fact that a 4.44 MeV bias had been introduced into the beta counter to cut off background activities. Consequently, the fractions of beta particles having energies above

the bias are different for the two decay branches. A correction factor ε must be applied to the yield of P3 before the branching ratio can be deduced from the relative yields between P3 and P1 + P2. With a calculated value of 1.02 for ε, which was obtained from a program by Bahcall (1965) to calculate the F-function (modification was made to include the cut off energy for the beta particles), the relative population is found to be

$$\frac{^{9}\text{Li} \rightarrow {}^{9}\text{Be}(2.78)}{^{9}\text{Li} \rightarrow {}^{9}\text{Be}(2.43)} = (9.4 \pm 1.5)\% .$$

The error is estimated from

a) correction factor ε, ($\pm 2\%$)

b) relative efficiency of the neutron counter, ($\pm 10\%$)

c) separation of the peak, ($\pm 11\%$)

d) the extrapolation of P1 to zero neutron energy, ($\pm 5\%$).

Also formed is the ratio of P2 + P3 to P1. It is found to be $(14.2 \pm 2.8)\%$, which will be compared with the result from the delayed alpha spectrum.

C) The Delayed Alpha Spectrum

With T_1 and T_2 set equal to 520 and 20 msec and with the spectrometer and the windows on ΔE and $E + \Delta E$ channels properly adjusted for ^{9}Li, a total of 5,341 gates were accumulated during a 12 hour run. A separate background run was also taken in a manner described in part II, section 6 and was then subtracted from the ^{9}Li

decay data. The sum of the first half and the second half of the delayed alpha spectrum is shown in figure 17. The energy scale is obtained from the ^{8}Li calibration. Two new results which cannot be deduced from the delayed neutron spectrum are presented in the following sections.

1) The Ground State Branch of the ^{9}Li Decay

The beta-neutron coincidence method is incapable of studying the decay branch of the ^{9}Li to the ground state of ^{9}Be, because of the lack of delayed neutrons. The situation is slightly different in the recoil-particle method. The very fact, that one knows the total number of parent ^{9}Li nuclei produced and the counting period after their decays during the run, makes the determination possible. The only remaining problem is the separation of the low energy tail from the betas to the ground state from the delayed alphas in the spectrum. Under the assumption that all the ^{9}Li nuclei decay at the center of the E detector and that the energy deposited by the 13.6 MeV ground state branch beta is proportional to the distance traveled inside the E detector, a crude estimation of the beta spectral shape was obtained.

$$\frac{dY}{dE_{\beta}} = \text{const.} \times \frac{1}{E_{\beta}^{2}} \quad .$$

Furthermore, from the kinematics the minimum energy that the two alphas can have from the break up of the 2.43 MeV state in ^{9}Be is one-ninth of its total break up energy, that is 95 keV. The sharp rise below this energy must be entirely due to the betas. Therefore,

the calculated $1/E_\beta^2$ spectrum (see figure 17) has been normalized to the data at this peak. Let

N_t = total number of counts in the delayed alpha spectrum,

N_β = estimated total beta counts,

N_o = total number of ^{9}Li nuclei produced, and

N_{eff} = the effective number of ^{9}Li nuclei decaying in the counting period (N_{eff} is related to N_o simply by

$$N_{eff} = N_o (e^{-T_2/\tau} - e^{-T_1/\tau}), \quad \text{where}$$

T_1 is the total beam off time, T_2 is the waiting period and τ is the mean life of ^{9}Li nucleus), the ground state branching ratio of the ^{9}Li beta decay is given by

$$\frac{N_{eff} - (N_t - N_\beta)}{N_{eff}} \quad \text{and}$$

is found to be $(65^{+2.4}_{-2.7})\%$. The error includes

a) uncertainty in N_β, ($\pm 30\%$)

b) statistical uncertainties, ($\pm 2\%$)

c) uncertainty in N_t, ($\pm 2\%$)

d) uncertainty in T_1, T_2 and τ, ($\pm 1\%$).

2) Comparison with the Neutron Spectrum

The delayed neutron spectrum and the delayed alpha spectrum are complementary to each other in the following sense. For a given break up of an excited state in ^{9}Be, the total energy available for the neutron and the two alphas is fixed. In view of this simple relation, the low energy portion of the delayed neutron spectrum, which suffers large errors due to the neutron bias, can always be supplemented by the high energy portion of the delayed alpha spectrum, or vice versa. Two such comparisons have been made and show the evident agreement between the two spectra.

a) The same calculated curve, which describes the break up of the 2.43 MeV state into the continuum fits the neutron spectrum as well as the delayed alpha spectrum (see figure 17).

b) The peak at approximately 180 keV and the enhancement above it in the delayed alpha spectrum correspond to the peaks P2 and P3 in the delayed neutron spectrum. Because of the rather poor statistics, no attempt has been made to separate P2 and P3 in the delayed alpha spectrum. However, the total number of counts in the peak region after the subtraction of the beta tail and the continuum was compared with the counts in the continuum. The ratio is found to be $(12.4 \pm 4.3)\%$, which is in good agreement with the $(14.2 \pm 2.8)\%$ from the delayed neutron spectrum.

As mentioned in section B, the continuous spectrum from the break up of the 2.43 MeV state in ^{9}Be into three particles is strongly modified by the Coulomb barrier penetration factor between the two alphas. Consequently the spectrum tends to peak at lower

neutron energy, where the two alphas have higher energies and the Coulomb penetration factor is larger. A similar result should be expected for the 2.78 MeV state in ^{9}Be. Because of the relatively weak population of the 2.78 MeV state relative to the 2.43 MeV state and the large uncertainty in the relative efficiency of the neutron detector for lower energies, no conclusion can be drawn about the continuous decay branch of the 2.78 MeV state from the delayed neutron spectrum. On the other hand, if the 2.78 MeV state does partly decay directly into three particles, there should be a continuum beyond the 860 keV (the end point energy for the break up of the 2.43 MeV state) in the delayed alpha spectrum. However, no clear enhancement is observed in this energy region. An upper limit of 50% is placed on this branching ratio. The rather large limit reflects the poor statistics. (The few counts observed beyond the end point for the 2.43 MeV state decay cannot be attributed to the continuum decay of the 2.78 MeV state, because they do not have the right half life. The few events seen are probably due to $^{8}Li^{++}$'s stopped in the ΔE detector and which give a very weak time-independent component.)

3) Decay Modes of ^{9}Li and Branching Ratios

From the results of previous analysis together with calculated values of the F-functions, branching ratios and log ft values of the ^{9}Li beta-decay to the ground state, the 2.43 and the 2.78 MeV states are found to be:

branching ratios $(65^{+2.7}_{-2.4})\%$, $(32^{+2.7}_{-3.7})\%$, $(3.0^{+2.7}_{-0.3})\%$ and

log ft values $(5.12^{+0.01}_{-0.02})$, $(5.00^{+0.04}_{-0.05})$, $(5.97^{+0.05}_{-0.28})$,

respectively.

IV. DISCUSSION

A) Rotational Model Interpretation

Since the spherical shell model does not allow the possibility of an f-wave decay of the 2.43 level to ^{8}Be(g.s.), configuration mixing must be involved. A successful treatment based on the Nilsson model has been given by Stephenson (1966). More specifically, the generating coordinate representation was used to include the major shell mixing effect. A large deformation, δ, of the order of 0.8 for the ^{9}Be ground state rotational band, was needed to account for the f-wave decay branching ratio. Therefore, it is of some interest to calculate the level scheme for low lying states in ^{9}Be by treating it as a deformed nucleus.

The basic physical idea of the rotational model involves the existence of a deformed nuclear shape, which provides a non-spherical field in which the individual nucleons move. Following the earlier work by Elliott (1958), the total nuclear Hamiltonian can be written as

$$H = H_{intr.}(x') + T_{rot.} + H_{coup.}$$

where $H_{intr.}$ is the intrinsic particle-Hamiltonian, x's are the intrinsic coordinates,

$T_{rot.}$ is the kinetic energy operator of the rotational motion, and

$H_{coup.}$ is the coupling between the intrinsic and rotational motions.

Denote $\vec{I}$ to be the total angular momentum, $\vec{J}$ to be the intrinsic angular momentum, $\vec{R}$ to be the angular momentum of the collective motion, and assuming the nuclear matter is a rigid, axially symmetrical top (z' is the axis of symmetry), $T_{rot.}$ is explicitly given by

$$T_{rot.} = \frac{\hbar^2}{2\mathcal{J}} \vec{R}^2 + \left(\frac{\hbar^2}{2\mathcal{J}_{z'}} - \frac{\hbar^2}{2\mathcal{J}} \right) R_{z'}^2$$

where $\mathcal{J} = \mathcal{J}_{x'} = \mathcal{J}_{y'}$ and $\mathcal{J}_{z'}$ are the corresponding moments of inertia. Or, replacing $\vec{R}$ by $\vec{I} - \vec{J}$, $T_{rot.}$ can also be written as

$$T_{rot.} = \frac{\hbar^2}{2\mathcal{J}} (\vec{I}^2 + \vec{J}^2 - 2(\vec{I} \cdot \vec{J})) + \left(\frac{\hbar^2}{2\mathcal{J}_{z'}} - \frac{\hbar^2}{2\mathcal{J}} \right)(I_{z'} - J_{z'})^2 .$$

Under the adiabatic assumption, the total wave function can be split into two parts – the intrinsic wave function $\chi_K(x')$ and the rotational wave function $D(\mathcal{J})$. The $H_{coup.}$ is assumed to be small compared to $H_{int.}$ and $T_{rot.}$. By demanding that the total wave function have a definite parity and reflection symmetry in the x' - y' plane, the properly normalized wave function is given by

$$\Psi(IKM) = \left(\frac{2I+1}{16\pi^2}\right)^{1/2} \{D^I_{M,K}(\mathcal{J})\, \chi_K(x') + (-1)^{I-J} D^I_{M,-K}(\mathcal{J})\, \chi_{-K}(x')\}$$

where K is the projection of the total angular momentum on the z' axis and M is the projection on the space fixed z axis. $D^j_{m,m'}(\mathcal{J})$ is the rotational function. Notice that the operator $\vec{I}$ only operates on D's and $\vec{J}$ only operates on χ_K. Although the intrinsic angular

momentum $\vec{J}$ is not a good quantum number, J_z, is a constant of motion because of the axial symmetry.

$$J_{z'} \psi = \Omega \psi \ .$$

The axial symmetry of the nuclear shape about the z' axis also requires

$$R_{z'} \psi = 0 \qquad \text{or}$$

$$I_{z'} D^{I}_{M,K}(\vartheta) = J_{z'} D^{I}_{M,K}(\vartheta)$$

which implies $K = \Omega$, and also

$$\left(\frac{\hbar^2}{2\mathcal{J}_{z'}} - \frac{\hbar^2}{2\mathcal{J}} \right) \left(I_{z'} - J_{z'} \right)^2 = 0 \ .$$

The wave function ψ is an eigenfunction for the Hamiltonian $\frac{\hbar^2}{2\mathcal{J}} \vec{I}^2$ with

$$\left(\frac{\hbar^2}{2\mathcal{J}} \vec{I}^2 \right) \psi = I(I+1) \frac{\hbar^2}{2\mathcal{J}} \psi$$

and for the term $H_{intr.}$ with

$$H_{intr.} \psi = E_{intr.} \psi \ .$$

The rest of the terms in H will be treated as perturbations. The terms $\frac{\hbar^2}{2\mathcal{J}} \vec{J}^2$ and $\frac{\hbar^2}{2\mathcal{J}} (-2(\vec{I}_{z'} \cdot \vec{J}_{z'}))$ give the same energy shift for all members within a given band, thus can be neglected within the band. However, they should be included in discussing the energy spacing for two different bands. The matrix elements are calculated as follows:

$$d = \frac{\hbar^2}{2\mathcal{J}} \langle \psi | \vec{J}^2 | \psi \rangle = \frac{\hbar^2}{2\mathcal{J}} \sum_J |C_J|^2 J(J+1), \text{ where } C_J \text{ is given by}$$

$$\chi_K(x') = \sum_J C_J \chi_K^J(x')$$

$$\langle \psi | \vec{I}_{z'} \cdot \vec{J}_{z'} | \psi \rangle = K \cdot \Omega = K^2 \quad .$$

The last term $\langle \psi | I_1' J_{-1}' + I_{-1}' J_1' | \psi \rangle$ is given by

$$\langle \psi | I_1' J_{-1}' + I_{-1}' J_1' | \psi \rangle = \frac{1}{2} a (-1)^{I+1/2} (I + \tfrac{1}{2}) \delta_{K, 1/2}$$

with $$a = \sum_J |C_J|^2 (-1)^{J-1/2} (J + 1/2) \quad .$$

At this point, an explicit model for the intrinsic motion has to be introduced in order to calculate the decoupling parameter 'a' and the matrix element d. Nilsson (1955) suggested the following form for the $H_{intr.}$:

$$H_{intr.} = \overset{o}{H}_o + H_\delta + C(\vec{\ell} \cdot \vec{s}) + D \vec{\ell}^2 \quad , \quad \text{where}$$

$\overset{o}{H}_o = \frac{\hbar\omega_o(\delta)}{2}(-\nabla_r^2 + r^2)$, and $\vec{r}$ is related to the intrinsic coordinates $\vec{r}'$ by $x = (M\omega_o/\hbar)^{1/2}x'$, etc.

$H_\delta = -\delta\hbar\omega_o(\delta)\frac{4}{3}\sqrt{\pi/5}\ r^2 Y_{20}$, where δ is a parameter characterizing the deformation

C = spin-orbit coupling strength

D = strength of the interaction giving a compromise between the harmonic oscillator potential and the square well potential.

The condition of constant volume of the nucleus gives

$$\omega_o(\delta) = \overset{o}{\omega}_o(1 - \frac{4}{3}\delta^2 - \frac{16}{27}\delta^3)^{-1/6}$$

, where $\overset{o}{\omega}_o$ is the value of $\omega_o(\delta)$ for $\delta = 0$. Instead of C, D and δ, a set of more convenient parameters were also used

$$k = \frac{-1}{2}\frac{C}{\overset{o}{\hbar\omega}_o} \quad , \quad \mu = \frac{2D}{C} \quad , \quad \eta = \frac{\delta}{k}\frac{\omega_o(\delta)}{\overset{o}{\omega}_o} \quad .$$

The base states chosen by Nilsson are diagonal in $\overset{o}{H}_o$ and are denoted by $|N\ell\Lambda\Sigma\rangle$, where N is the principal quantum number, ℓ is the orbital angular momentum, Λ is the magnetic quantum number and Σ is the spin projection along the body symmetric axis.

$$\overset{o}{H}_o\ |N\ell\Lambda\Sigma\rangle = (N + \frac{3}{2})\ \hbar\ \omega_o(\delta)$$

$$\Lambda + \Sigma = \Omega \ .$$

Neglecting the coupling between shells with N differing by 2, the Nilsson single-particle orbits for a given N and Ω are obtained by expanding the wave functions in terms of base states $|N \ell \Lambda \Sigma\rangle$ and diagonalizing the energy matrix elements. Denoting the eigenvalues for given N and Ω by $r^{N}_{\alpha\Omega}$, the total energy for a given orbit can be written as

$$E^{N\Omega}_{\alpha} = (N_{\alpha} + \frac{3}{2}) \hbar \omega_{o}(\delta) + k \hbar \overset{o}{\omega}_{o} r^{N\Omega}_{\alpha}(\eta) \ .$$

The proper value of $\hbar \overset{o}{\omega}_{o}$ is given by Nilsson as

$$\hbar \overset{o}{\omega}_{o} \sim 41 \times A^{-1/3} \text{ MeV} \ .$$

The wave function corresponding to each α is later used to calculate the decoupling parameter a and the energy matrix element d.

The Nilsson configuration for the ground state of ^{9}Be should consist of 4 particles in orbit #1 (N = 0, Ω = 1/2), 4 particles in orbit #3 (N = 1, Ω = 1/2) and 1 particle in orbit #2 (N = 1, Ω = 3/2). It has $J^{\pi} = 3/2^{-}$. The subsequent higher members in this rotational bands are identified as the 2.43 MeV state ($5/2^{-}$) and the 6.76 MeV state ($7/2^{-}$). The intrinsic wave function for the next higher rotational band should have the Nilsson configuration of 4 particles in orbit #1, 4 particles in orbit #3 and 1 remaining particle in orbit #4 (N = 1, Ω = 1/2). The lowest member should be a $J^{\pi} = 1/2^{-}$ state. The energy spacing between the $1/2^{-}$ state and the ground state is calculated with the following assumptions:

a) For large deformation Nilsson orbit #2 and #4 are degenerate and both belong to the N = 1, $n_{\perp} = 1$ configuration. It

is reasonable to assume that the K = 3/2 and the K = 1/2 bands have the same deformation. Further justification of this assumption is presented later as one calculates the f-wave reduced width of the 2.43 MeV state from this model. The deformation parameter η is chosen to be 12.

b) The spin-orbit interaction strength parameter k is chosen to be 0.08, which has been successfully used by Chesterfield and Spicer (1963) for the ^{7}Li nucleus and also provides the necessary energy splitting between the K = 1/2 and the K = 3/2 bands in ^{9}Be. A deformation parameter of 0.7 is implied for δ.

c) The parameter μ is set to zero, since the effect of the $D\vec{\ell}^2$ term is important only when N > 3.

d) $\hbar^2/2\mathcal{J}$ is determined to be 0.486 MeV from the energy spacing between the ground state and the 2.43 MeV state.

Explicit formulae for the eigenvalue $r_{\alpha}^{N\Omega}(\eta)$, the decoupling parameter a and the energy matrix elements for the orbit #2 and orbit #4 are given in Appendix II.

Also calculated are the energy spacings for states within the ground state band and the K = 1/2 band. The resultant level scheme is shown in figure 18. The three lowest members in the $1/2^-$ band are situated at 2.69 MeV ($1/2^-$), 4.99 MeV ($3/2^-$) and 6.00 MeV ($5/2^-$). The experimental value for the $1/2^-$ state is (2.78 $\pm$ 0.125) MeV. Thus, fair agreement can be obtained with this model.

As mentioned in Nilsson's paper, for large deformations, the wave function is very close to the generator coordinates representation. That is, instead of using the base vectors as $|N\ell\Lambda\Sigma\rangle$,

the product wave functions of three independent one-dimensional harmonic oscillators are used. In the present case of ^{9}Be nucleus, the Nilsson orbit #2 is a pure $|111 + 1/2\rangle$ configuration. The Nilsson orbit #4, for the large deformation of $\delta = 0.7$, contains 99% in amplitude of the configuration $|111 - 1/2\rangle$. Therefore, they both belong to the $N = 1$, $n_{\perp} = 1$ configuration in the generator coordinates. The spatial parts of the wave functions is essentially identical. As a result, the experimental p-wave reduced width for the 2.78 MeV state ($1/2^{-}$) can be used to deduce the f-wave reduced width for the 2.43 MeV state. Following the calculation by Stephenson with a slightly different definition for the deformation parameter α,

$$\frac{\theta_f^2}{\theta_p^2} = \left\{ \sqrt{2/5} \cdot \left[\tanh(\alpha) + \tanh\left(\frac{\alpha}{2}\right)\right] \right\}^2 ,$$

where α is related to δ by

$$\alpha = \frac{1}{2} \ell n\left(1 + \frac{2}{3}\delta\right) .$$

Using the deformation parameter $\delta = 0.7$ and the experimental value of the p-wave reduced width for the 2.78 MeV state

$$\theta_p^2 = 0.48 \text{ (in units of } \hbar^2/MR^2 = 2.47 \text{ MeV)},$$

the f-wave reduced width for the 2.43 MeV state is predicted to be

$$\theta_f^2 = 1.6 \times 10^{-2} .$$

It should be compared with the experimental value

$$\theta_f^2 = (2.1 \pm 0.6) \times 10^{-2}$$

found by Christensen and Cocke (1966) and confirmed by the present data.

B) Intermediate Coupling Shell Model Interpretation

The Nilsson model is most often applied to nuclear states with single particle intrinsic wave functions. However, this is not the case for the ^{9}Li ground state. Therefore, a theoretical estimate for the transition matrix elements of the ^{9}Li beta decay is carried out within the framework of an intermediate coupling shell model. All states involved are treated as $(1s)^4(1p)^5$ configurations. A recent calculation of this kind for light nuclei (A = 6 to 9) was given by Barker (1966). The effective interaction is taken as

$$V = \sum_{i<j} (W + MP_{ij}^{x} - HP_{ij}^{\tau} + BP_{ij}^{\sigma}) J(r_{ij}) + a \sum_i (\vec{l}_i \cdot \vec{s}_i)$$

where p^x, p^τ and p^σ are the space, isospin and spin exchange operators. A total of six independent parameters are involved; three exchange force mixing parameters, two radial integral parameters and the spin-orbit interaction strength parameter. The basic shell model states are taken as $[\lambda]^{2T+1,\ 2S+1}L$ in the L-S coupling scheme. For the A = 9 system, the parameters were chosen to fit the observed energy levels (including the postulated $1/2^-$ state at 2.4 MeV). The major part of the ground state, the

$1/2^-$ state and the $5/2^-$ state wave functions of ^{9}Be was found to be of $[41]^{22}P$, $[41]^{22}P$ and $[41]^{22}D$ configurations, as one expects from the extreme L-S coupling limit. The ground state of ^{9}Li (or the lowest $T = 3/2$ state in ^{9}Be) consists mostly of the $[32]^{42}P$ configuration. The allowed Gamow-Teller beta decay matrix element is calculated in the usual fashion:

$$\langle \sigma^2 \rangle = \frac{1}{2I_i + 1} \sum_{M_f M_i k} | \langle I_f M_f T_f M_{T_f} | \sum_{j=1}^{5} \sigma_k(j) \tau_+(j) | I_i M_i T_i M_{T_i} \rangle |^2$$

where σ_k are the Pauli spinors and τ_+ are the isospin raising operator. I_i, M_i, T_i, M_{T_i} and I_f, M_f, T_f, M_{T_f} are the total spin, z-projection of the spin, total isospin, z-projection of the isospin of the parent and daughter nuclei. The ft value is given by

$$ft = \frac{2\pi^3 \ell n 2 (\hbar/m_e c)^7 m_e^2 c^3 G^{-2}}{(C_A/C_V)^2 \langle \sigma^2 \rangle}$$

where m_e is the electron mass, c is the velocity of light and G is the weak interaction coupling constant.

The procedure of the calculation is, first of all, to expand the initial and final state wave functions as

$$\psi(I, T) = \sum_{[\lambda]LS} a^{[\lambda]LST} \phi(p^n, [\lambda]LST)$$

where $\phi(p^n, [\lambda]LST)$ are shell model basis states in the L-S coupling scheme, n is the number of nucleons in the 1p shell. The subscripts i and f of I and T have been dropped for simplicity. $a^{[\lambda]LST}$ are

amplitudes of the expansion. The second step is to expand $\phi(p^n, [\lambda]LST)$ as

$$\phi(p^n, [\lambda]LST) = \sum_{[\lambda_1]L_1S_1T_1} C^{[\lambda]LST}_{[\lambda_1]L_1S_1T_1} \phi(p^{n-1}, [\lambda_1]L_1S_1T_1)\, \chi_p$$

where $\phi(p^{n-1}, [\lambda_1]L_1S_1T_1)$ are the shell model basis states for (n-1) particles in the 1p shell, χ_p is the wave function for an 1p shell nucleon and $C^{[\lambda]LST}_{[\lambda_1]L_1S_1T_1}$ are the fractional parentage coefficients. At this point, the beta transition matrix elements involve only single-particle operators and can then be easily deduced. Details of this calculation are given in Appendix III.

Because of the specific shell model selection rule, the transition from [32] to [41] configurations is strictly forbidden. As a result, the matrix elements become very sensitive to the small components in the wave functions. The predicted log ft values from Barker's wave functions are 5.32, 5.31 and 5.38 for the ground state, the $5/2^-$ and the $1/2^-$ states branches respectively. The comparison between theoretical and experimental results is given in table 1. The present experimental result of $5.97^{+0.05}_{-0.28}$ for the 2.78 MeV state seems to be higher than predicted, nevertheless, it is still consistent with a negative parity assignment for this state.

Also calculated is the p-wave neutron reduced width for the 2.78 MeV state. Barker's wave functions for the $1/2^-$ state in ^{9}Be and the ground state of ^{8}Be are used. (The explicit formula for the reduced width is given in Appendix III.) It is found to be 0.43 in units of $\hbar^2/MR^2$(=2.47 MeV). The present experimental value is 0.48 ± 0.06 (see part III, section B).

C) Conclusions

From the delayed neutron spectrum following the ^{9}Li beta decay, a group of neutrons corresponding to the break up of a state at an excitation energy of 2.78 MeV in ^{9}Be is clearly seen. Both the intermediate coupling shell model and the rotational model predict the existence of a $J^{\pi} = 1/2^{-}$ state at an excitation energy between 2 and 3 MeV and the second $3/2^{-}$ state well above 3 MeV. This result together with the fact that all the beta decay branches are allowed transitions, a $1/2^{-}$ assignment for the 2.78 MeV state is favored. This state decays mainly by emitting a p-wave neutron to the ground state of ^{8}Be.

Further improvement in the sensitivity of the time-of-flight neutron spectrometer may be useful to locate other lower members in the K = 1/2 band of ^{9}Be. It is also of great interest to study the delayed proton spectrum of the analog states in ^{9}B following the beta decay of ^{9}C with the recoil-particle method.

APPENDIX I. Determination of the Bias of the Neutron Detector

The neutron energy bias introduced by the internal discriminator of the start side of the TAC has been examined in the following manner:

The ZrT target was bombarded with a 2 MeV proton beam from the CIT-ONR tandem. The mono-energetic neutrons from the reaction $T(p,n)^3He$ were observed at 0^o with the neutron counter. The linear signal from the counter was amplified and analyzed with a 400 channel RIDL analyzer. The fast signal was sent to the start side of the TAC through a 50Ω impedance attenuator, this signal was also split off through a 1000Ω resistance into the linear amplifier on a 581 Tektronics Oscilloscope. The positive gate out on the scope was inverted with a pulse transformer and provided the stop signal for the TAC. The output from the TAC was then sent through an Ortec timing single channel analyzer, whose logic output was used as a gate to the RIDL analyzer. The gain of the linear amplifier on the 581 scope was set to a very sensitive scale (10mv/cm) such that there is always a stop signal for every neutron detected by the counter.

The procedure was then the following:

a) With no (0db) attenuation on the start side, a neutron spectrum gated by the TAC was taken. The position of the observed neutron knee corresponding to the full energy recoil protons was recorded.

b) With xdb attenuation on the start side, again a neutron spectrum gated by the TAC was taken. However, because of the attenuation, some of the recoil protons can no longer trigger the

TAC. Consequently, a lower cut off was observed in the neutron spectrum.

c) The neutron energy corresponding to this cut off after the corrections for the attenuation and the effect of having an extra branch of the fast signal to the oscilloscope (which normally did not exist when data were taken), gives the desired neutron bias.

This procedure was repeated several times with different attenuations, the averaged neutron bias was found to be (80 ± 20) keV.

APPENDIX II. Nilsson's Model Calculations

In the Nilsson model, the intrinsic wave function for a given band is expressed as

$$\chi_K^N(x') = \sum_{\ell\,\Lambda(\Sigma)} a_{\ell\,\Lambda(\eta)}\,|N\,\ell\,\Lambda\Sigma\rangle \qquad \text{with}$$

$$\Lambda + \Sigma = \Omega = K, \qquad \Sigma = \pm\frac{1}{2}$$

where N is the principal quantum number, ℓ is the orbital angular momentum, Λ, Σ and Ω are the projections of the orbital angular momentum, spin and the total angular momentum on the body z' axis. η is the deformation parameter. One can also expand $\chi_K^N(x')$ as

$$\chi_K^N(x') = \sum_{\ell\,\Lambda(\Sigma)} a_{\ell\,\Lambda} \sum_J (\ell\,\tfrac{1}{2}\,\Lambda\Sigma|JK)\,|N\ell JK\rangle$$

$$= \sum_J \Big[\sum_{\ell\,\Lambda(\Sigma)} a_{\ell\,\Lambda}(\ell\,\tfrac{1}{2}\,\Lambda\Sigma|\,JK)\Big]\,|N\,\ell\,JK\rangle$$

$$= \sum_J C_J\,|N\,\ell\,JK\rangle \qquad \text{with}$$

$$C_J = \sum_{\ell\,\Lambda\,(\Sigma)} a_{\ell\,\Lambda}(\ell\,\tfrac{1}{2}\,\Lambda\Sigma\,|\,JK)$$

where $(\ell\,\frac{1}{2}\,\Lambda\Sigma\,|\,JK)$ are the Clebsch-Gordon coefficients.

For Nilsson's orbit #2 (N = 1, $\Omega = K = 3/2$)

$$\chi(x') = a_{11} \,|111+\rangle \quad \text{with} \quad a_{11} = 1 \,.$$

The corresponding energy eigenvalue $r^{N}_{\Omega\alpha}$ is given by

$$r = \frac{1}{3}\eta - 1 \,.$$

For Nilsson's orbit #4 (N =1, $\Omega = K = 1/2$)

$$\chi(x') = a_{10} \,|110+\rangle + a_{11} \,|111-\rangle$$

$$r = \frac{1}{2}\left[\left(1 - \frac{1}{3}\eta\right) + \left(\eta^2 + 2\eta + 9\right)^{1/2}\right]$$

$$a_{10} = -\frac{\sqrt{2}}{\sqrt{\left(r + \frac{2}{3}\eta\right)^2 + 2}} \quad \text{and} \quad a_{11} = \frac{r + \frac{2}{3}\eta}{\sqrt{\left(r + \frac{2}{3}\eta\right)^2 + 2}} \,.$$

For the $K = 1/2^-$ band with Nilsson's orbit #4 as the intrinsic wave function, the decoupling parameter a is given by

$$\begin{aligned} a &= \sum_J (-1)^{J-1/2}\left(J + \tfrac{1}{2}\right) |C_J|^2 \\ &= \sum_J (-1)^{\ell} \left(a^2_{\ell 0} + 2\sqrt{\ell(\ell+1)}\; a_{\ell 0}\, a_{\ell 1}\right) \\ &= -\left(a^2_{10} + 2\sqrt{2}\; a_{10} a_{11}\right) \,. \end{aligned}$$

The energy matrix element d can be expressed as

$$d = \frac{\hbar^2}{2\mathcal{J}} \langle\chi|\vec{J}^2|\chi\rangle = \frac{\hbar^2}{2\mathcal{J}} \sum_J |C_J|^2 \; J(J+1)$$

$$= \frac{\hbar^2}{2\mathcal{J}} \sum_\ell (\ell + \tfrac{1}{2}) [\frac{a_{\ell 0}^2}{2\ell+1} (2\ell^2 + 2\ell + \tfrac{3}{2}) + 4a_{\ell 1}a_{\ell 0} \frac{\sqrt{\ell(\ell+1)}}{2\ell+1}$$

$$+ \frac{a_{\ell 1}^2}{2\ell+1} (2\ell^2 + 2\ell - \tfrac{1}{2})]$$

$$= \frac{\hbar^2}{2\mathcal{J}} (\frac{7}{4} + a_{10}^2 + 2\sqrt{2} \; a_{10}a_{11}) \; .$$

For the $K = 3/2^-$ band with Nilsson's orbit #2 as the intrinsic wave function, the energy matrix element d is given by

$$d = \frac{\hbar^2}{2\mathcal{J}} \sum_J |C_J|^2 \; J(J+1) = \frac{\hbar^2}{2\mathcal{J}} \frac{15}{4} \; .$$

Assuming that the $K = 1/2$ and $K = 3/2$ bands have the same deformation, the energy spacing between the lowest member of the two bands can be expressed as

$$\Delta E = [\frac{3}{2} (1 - \frac{1}{3}\eta) + \frac{1}{2} (\eta^2 + 2\eta + 9)^{1/2}] \hbar \overset{o}{\omega}_o k$$

$$+ \frac{\hbar^2}{2\mathcal{J}} [2(a_{10}^2 + 2\sqrt{2} \; a_{10}a_{11}) - 1]$$

with a_{10} and a_{11} as the expansion amplitudes for Nilsson's orbit #4.

APPENDIX III. Calculations of the ft Value and the Reduced Width

The procedure for the calculation of the Gamow-Teller beta transition matrix element in the framework of the intermediate coupling shell model is outlined in part IV, section B of the text. An explicit formula for $\langle \sigma^2 \rangle$ can be written as

$$\langle \sigma^2 \rangle = 18\, n^2 (2I_f+1)(2T_f+1)(2T_i+1) \begin{pmatrix} T_f & 1 & T_i \\ -M_{T_f} & q & M_{T_i} \end{pmatrix}^2$$

$$\times \left[\sum_{\substack{[\lambda_i] L_i S_i \\ [\lambda_f] L_f S_f}} \delta_{L_i L_f}\, a^{[\lambda_f] L_f S_f T_f}\, a^{[\lambda_i] L_i S_i T_i} \right.$$

$$\times \sqrt{(2S_f+1)(2S_i+1)} \begin{Bmatrix} S_f & I_f & L_f \\ I_i & S_i & 1 \end{Bmatrix} (-1)^{2S_f + L_f}$$

$$\times \Bigg(\sum_{[\lambda_1] L_1 S_1 T_1} C^{[\lambda_f] L_f S_f T_f}_{[\lambda_1] L_1 S_1 T_1}\, C^{[\lambda_i] L_i S_i T_i}_{[\lambda_1] L_1 S_1 T_1}$$

$$\left. \times (-1)^{S_1 + T_1} \begin{Bmatrix} \frac{1}{2} & S_f & S_1 \\ S_i & \frac{1}{2} & 1 \end{Bmatrix} \begin{Bmatrix} \frac{1}{2} & T_f & T_1 \\ T_i & \frac{1}{2} & 1 \end{Bmatrix} \Bigg) \right]^2$$

where n is the number of lp shell nucleons, I, T, M_T are the total angular momentum, isospin and z-projection of the isospin for the states, $[\lambda]$, L, S, T are the partition, total orbital angular momentum, spin and isospin of the shell model basis states for n particles in the lp shell. $a^{[\lambda] LST}$ are amplitudes of the expansion.

Subscripts i and f refer to the initial and final state wave functions. $C^{[\lambda]LST}_{[\lambda_1]L_1S_1T_1}$ are the fractional parentage coefficients given by Jahn, et al. (1951) and modified by Elliott, et al. (1953), with $[\lambda_1]L_1S_1T_1$ denoting the shell model basis states for (n-1) particles in the 1p shell. δ is the Kronecker delta symbol. The ft value is given by

$$ft = \frac{2\pi^3 \ell n 2(\hbar/m_e c)^{+7} m_e^2 c^3 G^{-2}}{(C_A/C_V)^2 \langle \sigma^2 \rangle} = \frac{\alpha}{\langle \sigma^2 \rangle} .$$

The numerical value for α is chosen to be

$$\alpha = 4700 .$$

The p-wave rediced width for states in ^{9}Be can be expressed as

$$\theta_p^2 = \frac{\hbar^2}{MR^2} \; s \; \theta^2_{s.p.}$$

with s given by

$$s = \sum_f | \sqrt{n} \; (T_1 \; \tfrac{1}{2} M_{T_1} \; M_T - M_{T_1} | T M_T)$$

$$\times \sum_{\substack{[\lambda]LS \\ [\lambda_1]L_1S_1}} (a^{[\lambda]LST} \; a^{[\lambda_1]L_1S_1T_1} \; C^{[\lambda]LST}_{[\lambda_1]L_1S_1T_1}$$

$$\times \sqrt{(2f+1)(2S+1)(2L+1)(2I_1+1)}$$

$$\times (-1)^{I_1+2f+2L_1+I+\frac{3}{2}} \begin{Bmatrix} L_1 & S_1 & I_1 \\ \frac{1}{2} & f & S \end{Bmatrix} \begin{Bmatrix} S & L_1 & f \\ 1 & I & L \end{Bmatrix} \Big)^2$$

where I, T, M_T are the total angular momentum, isospin and z-projection of the isospin for states in ^{9}Be; I_1, T_1, M_{T_1} are the similar quantities for states in ^{8}Be. The rest of the symbols have the same meaning as given previously.

The single-particle reduced width $\theta^2_{s.p.}$ for the 1p-shell nucleon is taken to be 0.6 (see Barker 1966). In the L-S coupling limit, the spectroscopic factor s for the transition from the $1/2^-$ (2.78 MeV) state in ^{9}Be to the ground state of ^{8}Be is given by

$$s\left[\psi_{^9\mathrm{Be}}(I=1/2^-,\ 41\ ^{22}P) \rightarrow \psi_{^8\mathrm{Be}}(I=0^+,\ 4\ ^{11}S)\right] = \frac{2}{3}.$$

For Barker's wave functions, it has the value

$$s = 0.72 .$$

REFERENCES

Alburger, D. E., 1963, Phys. Rev. 132, 328.

Alburger, D. E., et al., 1963, Phys. Rev. 132, 334.

Bahcall, J. N., 1965, Nucl. Phys. 75, 10.

Barber, W. C., Berthod, F., Fricke, G., Gudden, F. E., 1960, Phys. Rev. 120, 2081.

Barker, F. C., 1966, Nucl. Phys. 83, 418.

Bouten, M. Bouton, M. C., Depuydt, H., Schotsmas, L., 1969, Nucl. Phys. A127, 177.

Chen, Y. S., Nagatani, K., Tombrello, T. A., 1968, Bull. Am. Phys. Soc. 13, 1654.

Chesterfield, C. M., Spicer, B. M., 1963, Nucl. Phys. 41, 675.

Christensen, P. R., Cocke, C. L., 1966, Nucl. Phys. 89, 656.

Clerc, H. G., Wetzel, K. J., Spamer, E., 1968, Nucl. Phys. A120, 441.

Cocke, C. L., 1967, Ph.D. thesis, California Institute of Technology.

Cohen, S., Kurath, D., 1965, Nucl. Phys. 73, 1.

Edge, R. D., Peterson, G. A., 1962, Phys. Rev. 128, 2750.

Elliott, J. P., 1958, Univ. of Rochester NYO-2271.

Elliott, J. P., Hope, J., Jahn, H. A., 1953, Phil. Trans. Roy. Soc. A246, 241.

Jahn, H. A., et al., 1951, Proc. Roy. Soc. A209, 502.

Katz, L., Penford, A. S., 1952, Rev. Mod. Phys. 24, 28.

Kurath, D., 1956, Phys. Rev. 101, 216.

Lauritsen, T., Ajzenberg-Selove, F., 1966, Nucl. Phys. 78, 1.

Macefield, B.E.F., Wakefield, B., Wilkinson, D. H., 1969, Nucl. Phys. A131, 250.

Nefkens, B.M.K., 1963, Phys. Rev. Lett. 10, 243.

Nettles, P. H., Hensley, D. C., Tombrello, T. A., 1969, the Asilomar Conf. on Nuclear Isospin.

Ngoc, N. H., Hors, M., Perez y Jorba, J., 1963, Nucl. Phys. 42, 62.

Nilsson, S. G., 1955, Mat. Fys. Medd. Dan. Vid. Selsk. 29, No. 16.

Phillips, T. W., 1968, MIT Report 2098-330.

Schrank, G., Warburton, E. K., Daehnick, W. W., 1962, Phys. Rev. 127, 2159.

Schuster, N. A., Pake, G. E., 1951, Phys. Rev. 81, 886.

Stephenson, Jr., G. J., 1966, Int. Conf. on Nucl. Phys. Gatlinburg, Tennessee.

Summers-Gill, R. G., 1958, Phys. Rev. 109, 1591.

Taschek, R., 1948, Phys. Rev. 74, 373.

Tautfest, G. W., 1958, Phys. Rev. 110, 708.

Tombrello, T. A., 1966, Phys. Letts. 23, 134.

TABLE 1

The log ft values for the allowed Gamow-Teller beta decay of the ^{9}Li nucleus.

Column A; Cohen and Kurath, 1965.

Column B; Barker, 1966.

Column C; Alburger, 1963 and Macefield, 1969.

Column D; Present experiment.

Excitation energy in ^{9}Be	J^{π}, T	Theoretical Predictions A	B	Experimental Results C	D
g.s.	$\frac{3}{2}^{-}, \frac{1}{2}$	5.12	5.32	5.5 ± 0.2	$5.12^{+0.01}_{-0.02}$
2.43	$\frac{5}{2}^{-}, \frac{1}{2}$	5.10	5.31	4.8 ± 0.2	$5.00^{+0.04}_{-0.05}$
2.78	$\frac{1}{2}^{-}, \frac{1}{2}$	5.38	5.38	5.2 ± 0.2	$5.97^{+0.05}_{-0.28}$
-	$\frac{3}{2}^{-*}, \frac{1}{2}$	6.65	5.07	-	-

FIGURE 1

The energy level diagram of the ^{9}Be nucleus (Lauritsen and Ajzenberg-Selove, 1966). The state marked by * is established by the present ^{9}Li decay experiment. It has an excitation energy of 2.78 MeV ($J^{\pi} = 1/2^{-}$).

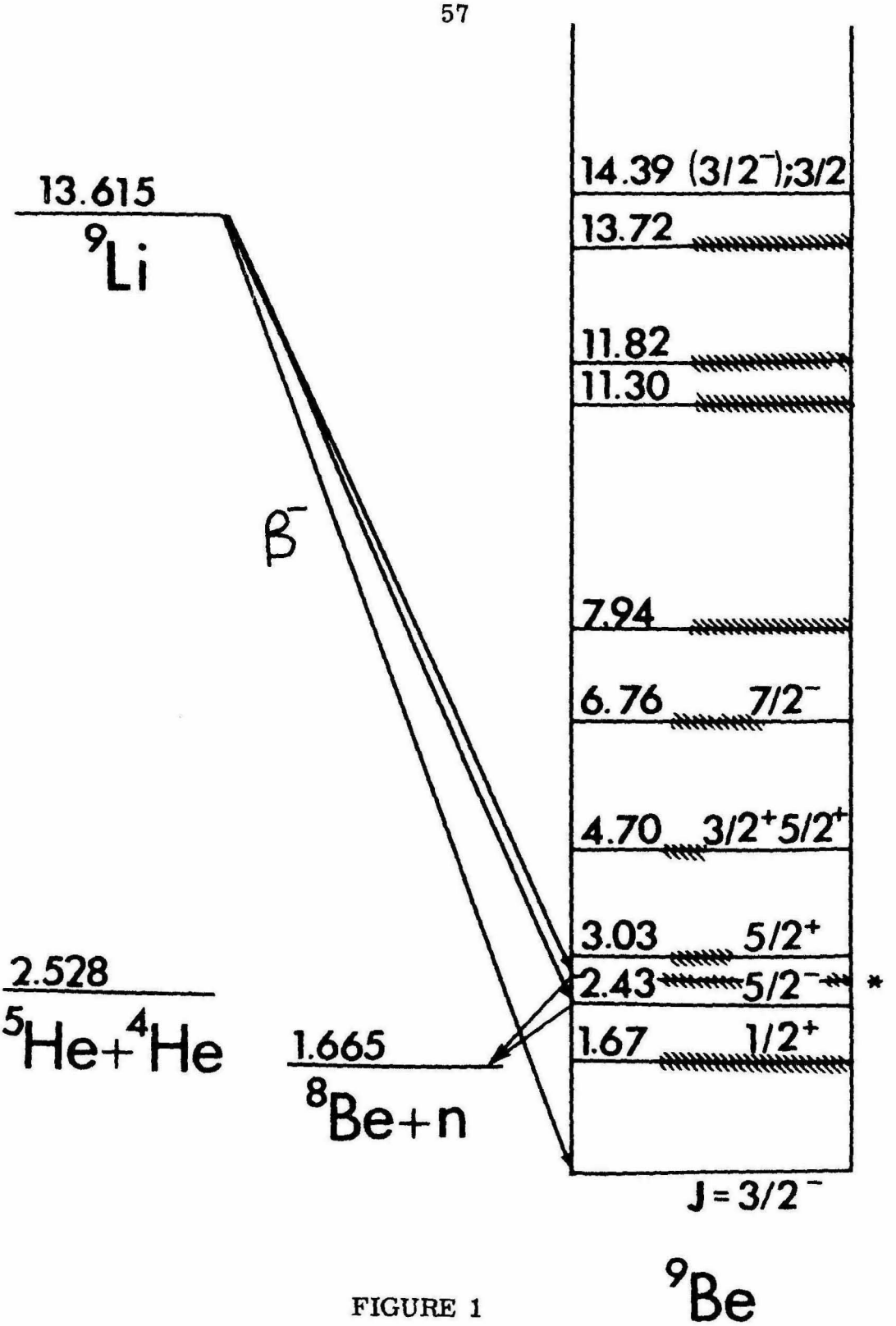
13.615
^{9}Li
β⁻
2.528
^{5}He+^{4}He
1.665
^{8}Be+n
14.39 (3/2⁻);3/2
13.72
11.82
11.30
7.94
6.76 7/2⁻
4.70 3/2⁺5/2⁺
3.03 5/2⁺
2.43 5/2⁻ *
1.67 1/2⁺
J = 3/2⁻
^{9}Be

FIGURE 1

FIGURE 2

The detector assembly at the focal point of the spectrometer.

A - Liquid nitrogen trap.

B - Copper rod kept at dry ice temperature. It is in thermal contact with the counter holder.

C - $\Delta E \times E$ counter telescope.

D - Brass shield in thermal contact with the liquid nitrogen trap.

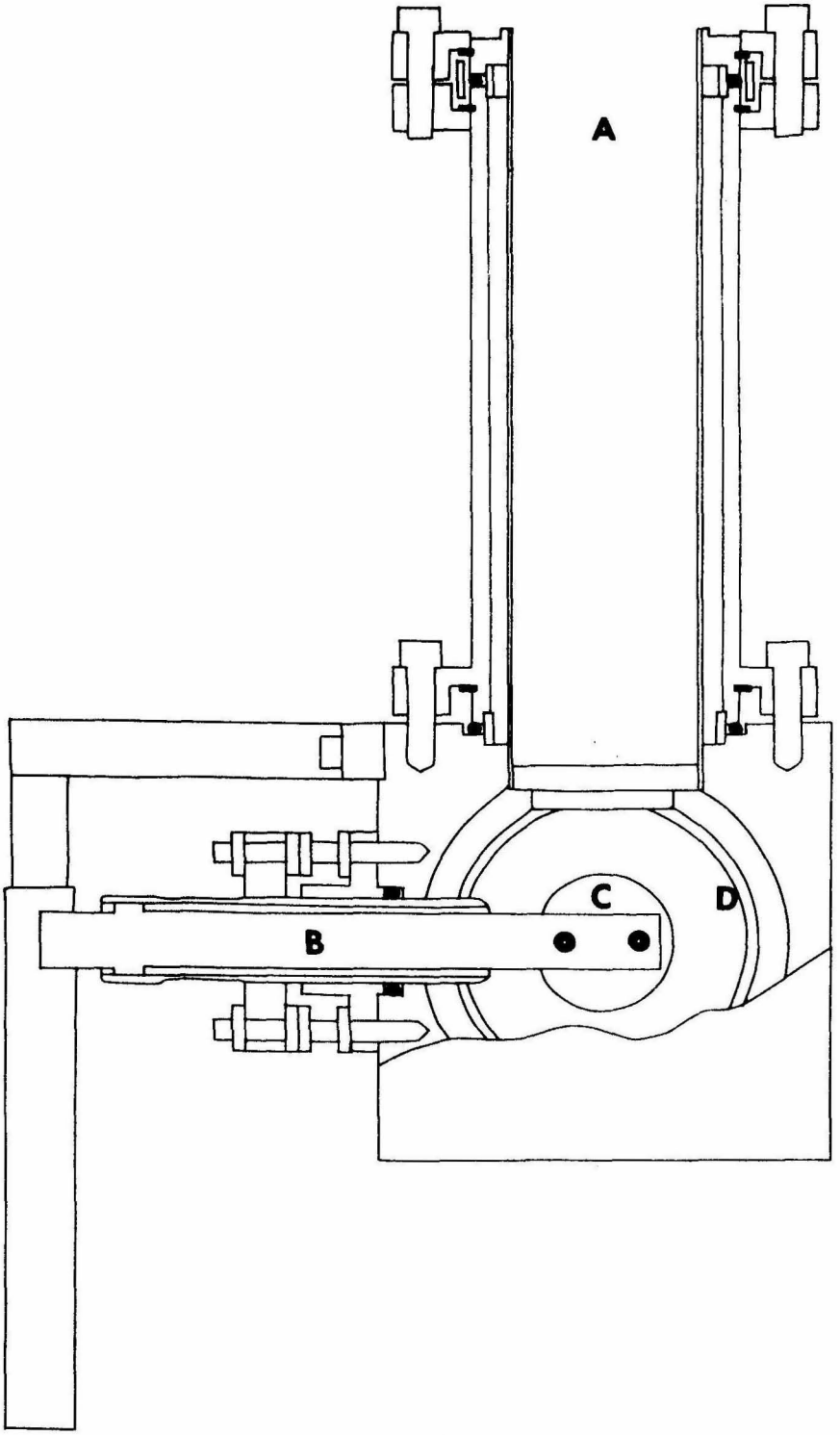

FIGURE 2

FIGURE 3

Particle identification system

S. C. A. - Ortec model 400 timing single channel analyzer.

Preamplifier - Tennelec model 100A.

Linear amplifiers - Ortec model 410 or RIDL model 30-23.

Slow coincidence and linear gate - Ortec model 409.

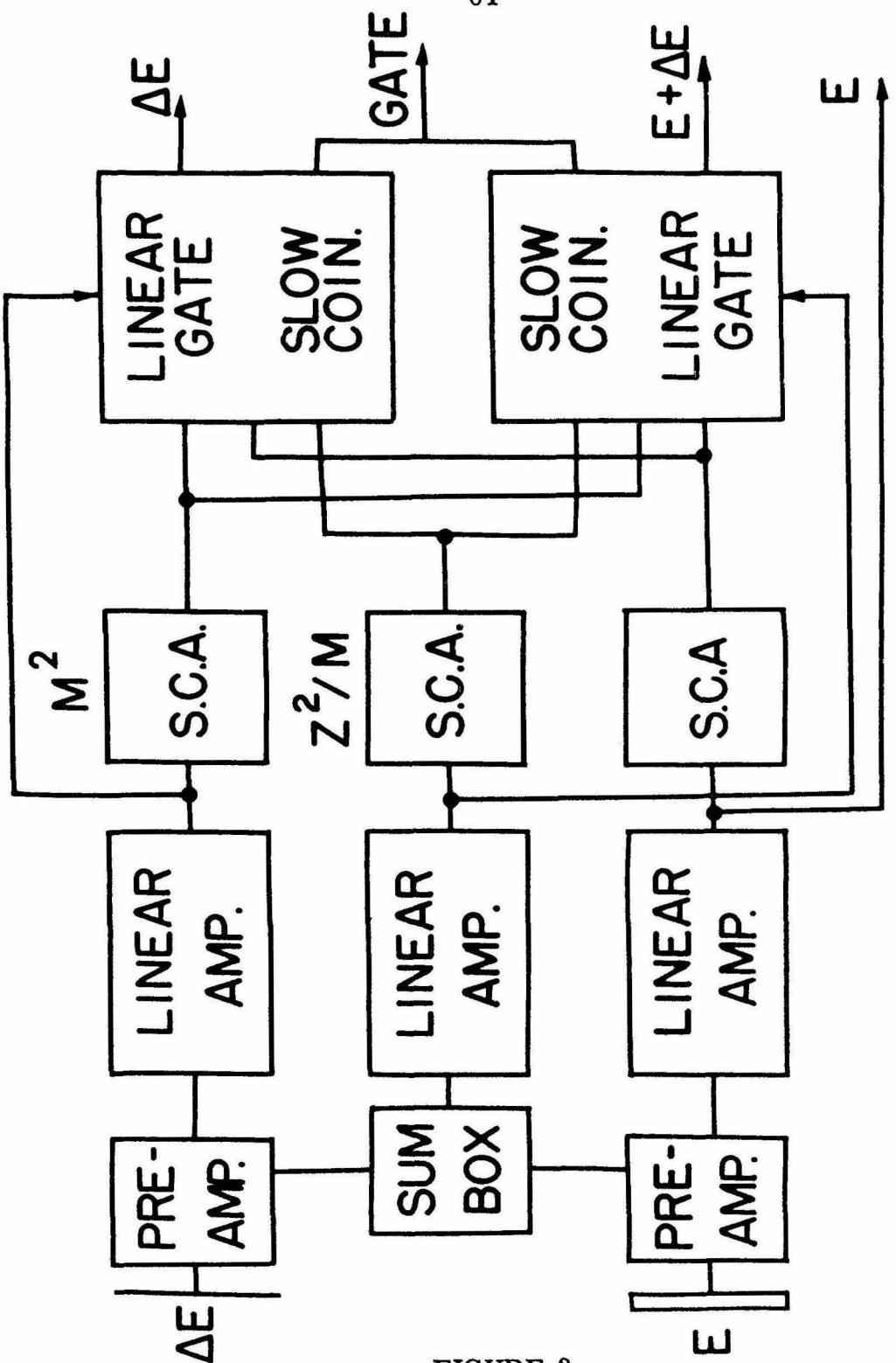
ΔE
GATE
E+ΔE
E
LINEAR GATE
SLOW COIN.
SLOW COIN.
LINEAR GATE
M²
S.C.A.
Z²/M
S.C.A.
S.C.A
LINEAR AMP.
LINEAR AMP.
LINEAR AMP.
PRE-AMP.
SUM BOX
PRE-AMP.
ΔE
E

FIGURE 3

FIGURE 4

Schematic diagram of the experimental procedure for the recoil-particle method (see text on page 8).

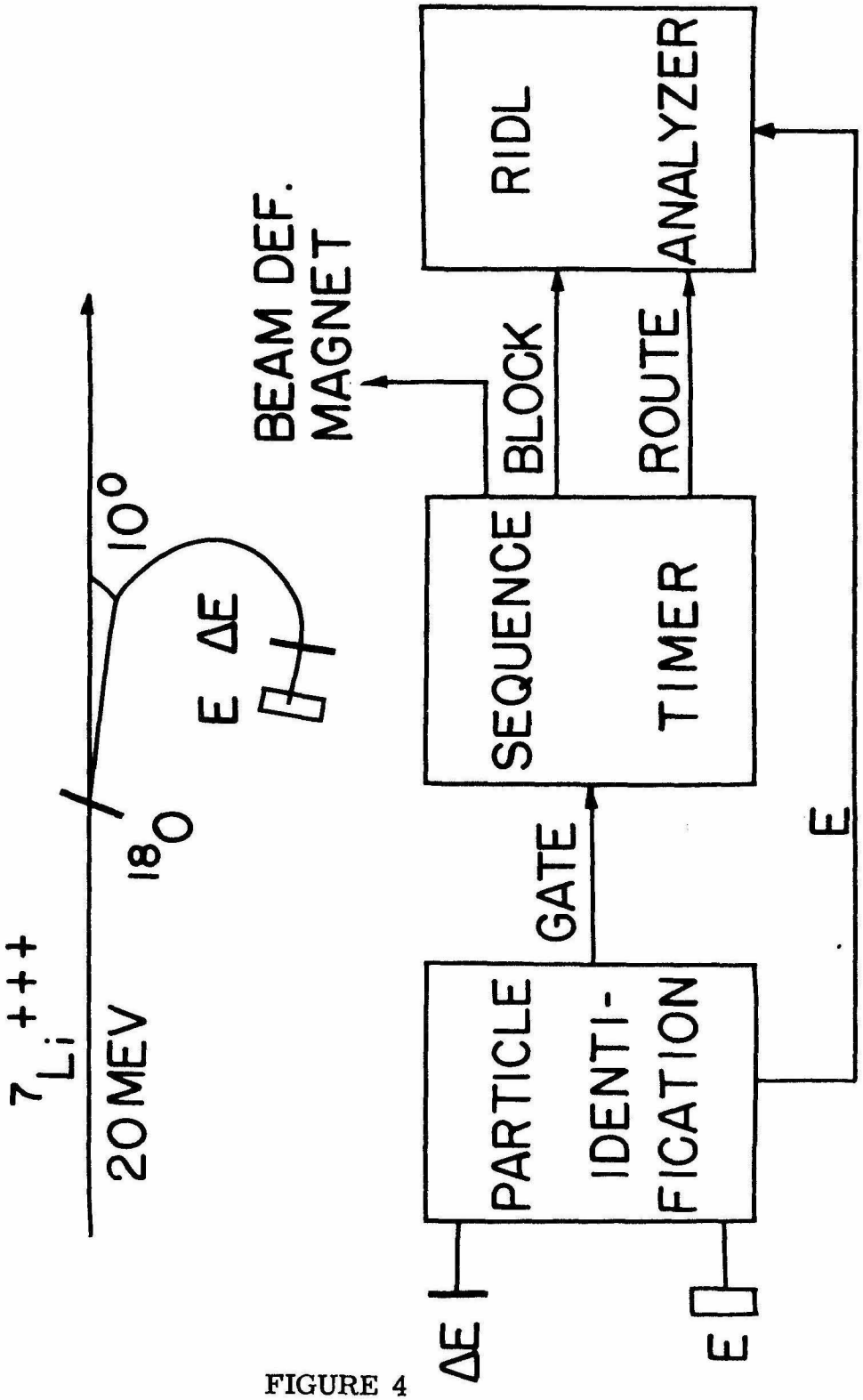
$^{7}Li^{+++}$
20 MEV
^{18}O
10°
E ΔE
BEAM DEF. MAGNET
RIDL ANALYZER
BLOCK
ROUTE
SEQUENCE TIMER
GATE
PARTICLE IDENTI-FICATION
E
ΔE
E

FIGURE 4

FIGURE 5

The delayed alpha spectrum of the ^{8}Li nucleus taken with the recoil-particle method.

The solid curve represents data from Alburger, et al. (1963).

The enhancement at 5 MeV indicates the delayed alpha particles were not being stopped inside the E detector. This gives an experimental estimation of the range for 13.65 MeV $^{8}Li^{+++}$ ions in silicon. The peak at 3 MeV provided an energy calibration for the E counter.

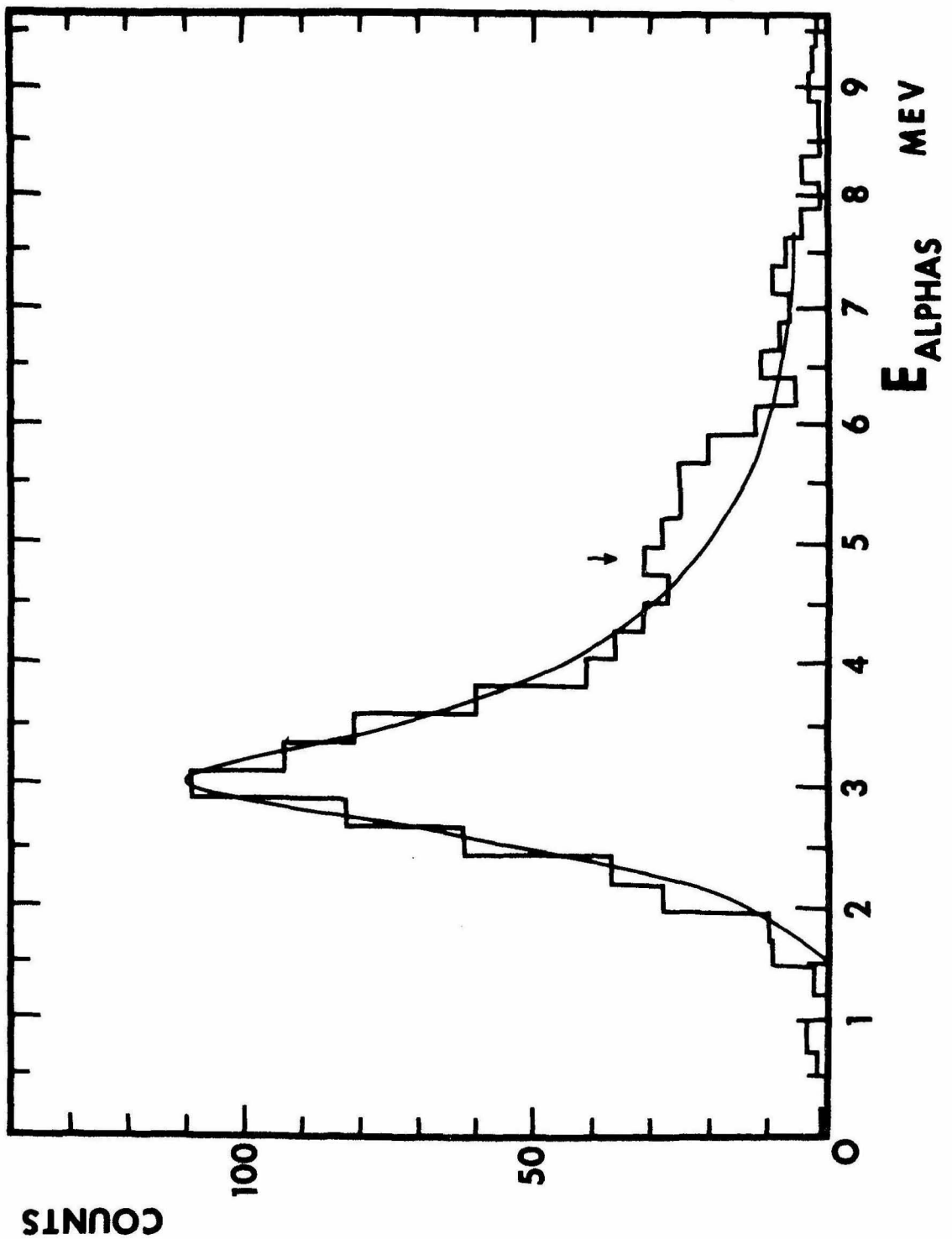

FIGURE 5

FIGURE 6

Electronic block diagram of the time-of-flight neutron spectrometer.

P.M. - photo multiplier tube.

P.A. - preamplifier.

L.A. - linear amplifier.

S.C.A. - timing single channel analyzer.

T.A.C. - time-to-pulse height converter.

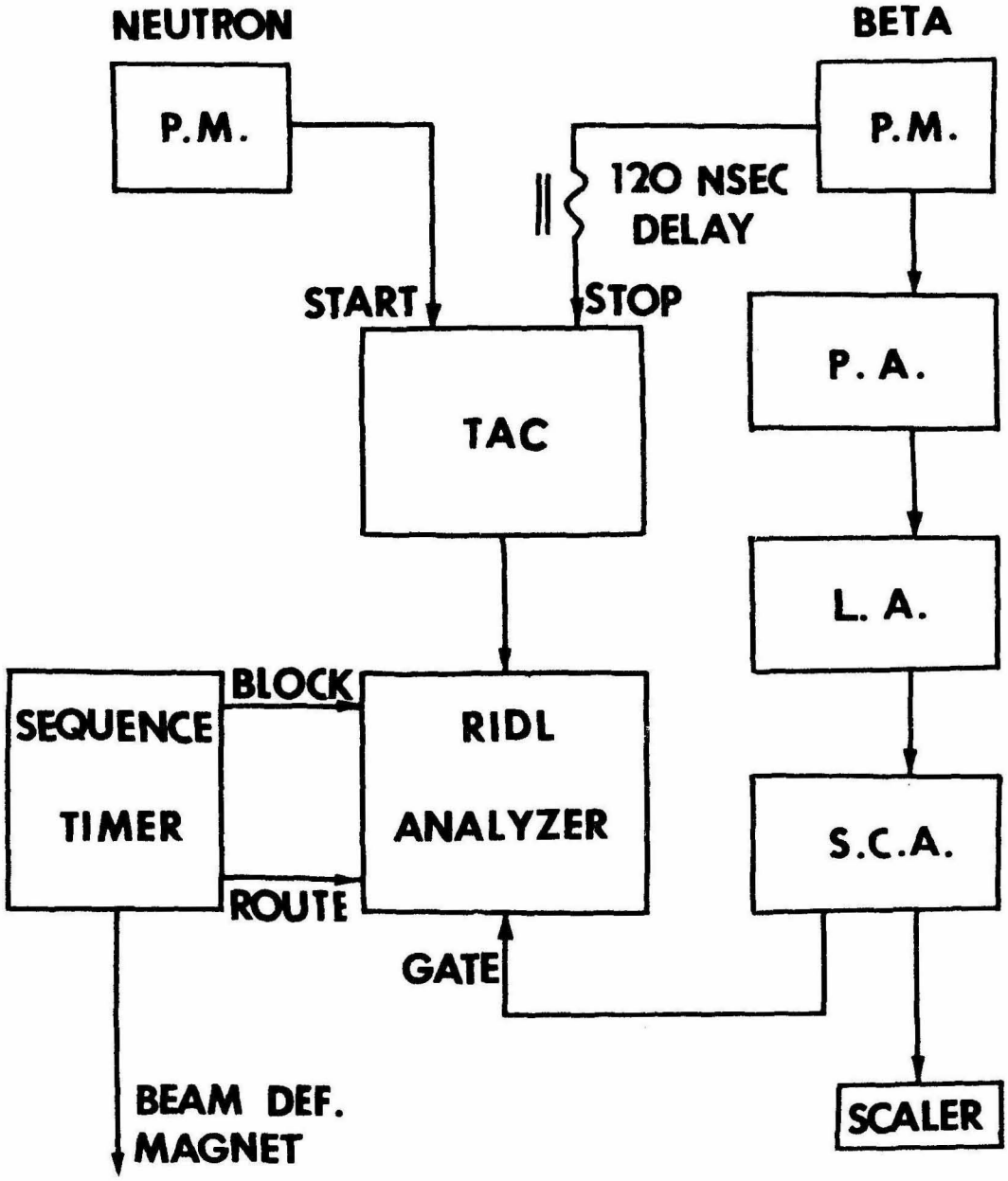
NEUTRON
P.M.
BETA
P.M.
120 NSEC
DELAY
START
STOP
TAC
P. A.
L. A.
S.C.A.
SEQUENCE
TIMER
BLOCK
ROUTE
RIDL
ANALYZER
GATE
BEAM DEF.
MAGNET
SCALER

FIGURE 6

FIGURE 7

Cable calibration of the time-of-flight neutron spectrometer. The coincidence γ-γ peak from the ^{22}Na source was used as the time reference. Data points were obtained by inserting different length RG58 cables into the start side of the TAC. The absolute time scale is found to be 0.641 nsec/channel.

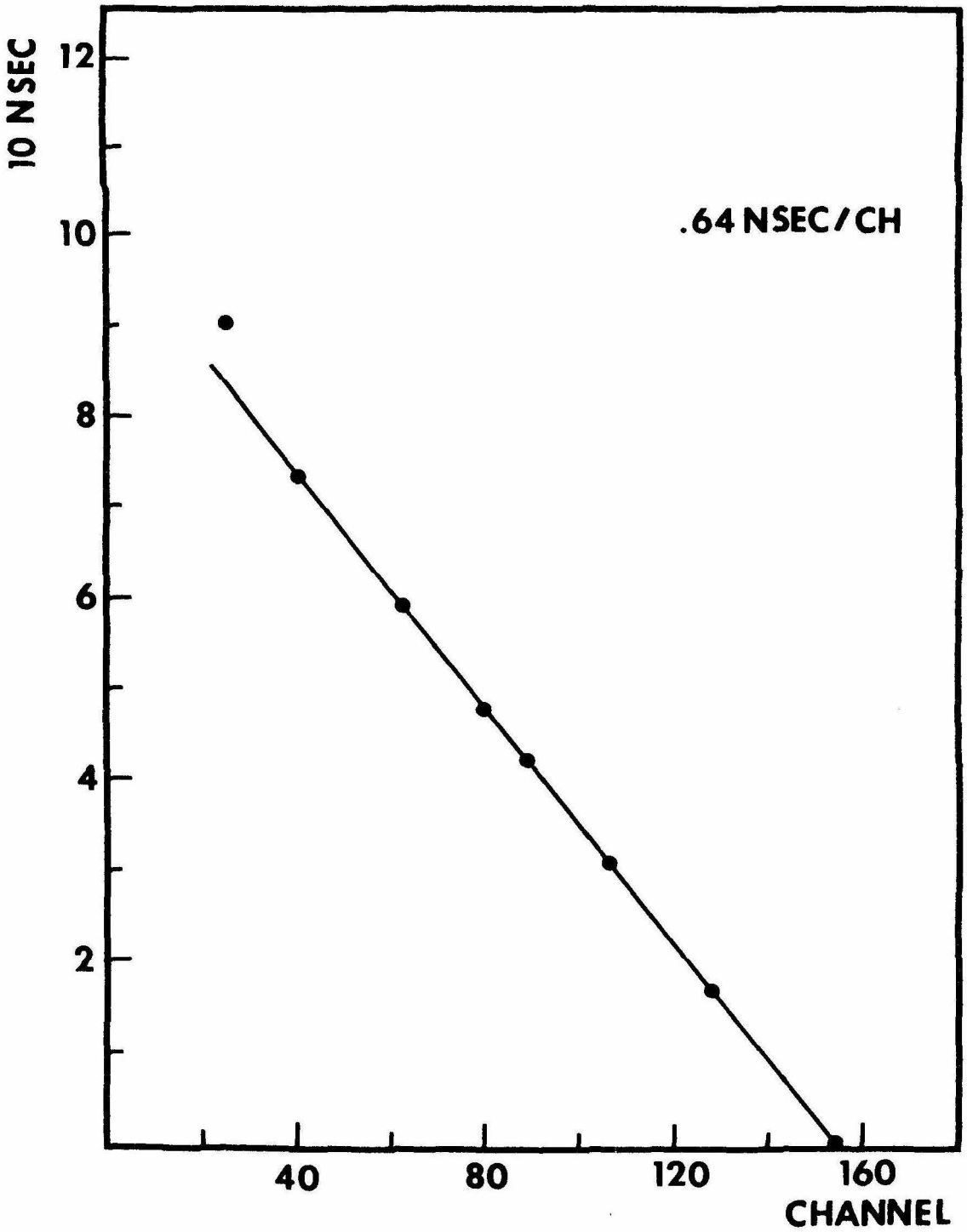

FIGURE 7

FIGURE 8

Random time spectrum of the time-of-flight spectrometer.

It was taken by placing a ^{22}Na source at the target position and a ^{137}Cs source in front of the neutron counter with 6" lead bricks in between. The result of a flat spectrum shows the linearity of the TAC. The peak near channel 150 is due to real coincidences from scattered γ-rays from the ^{22}Na source.

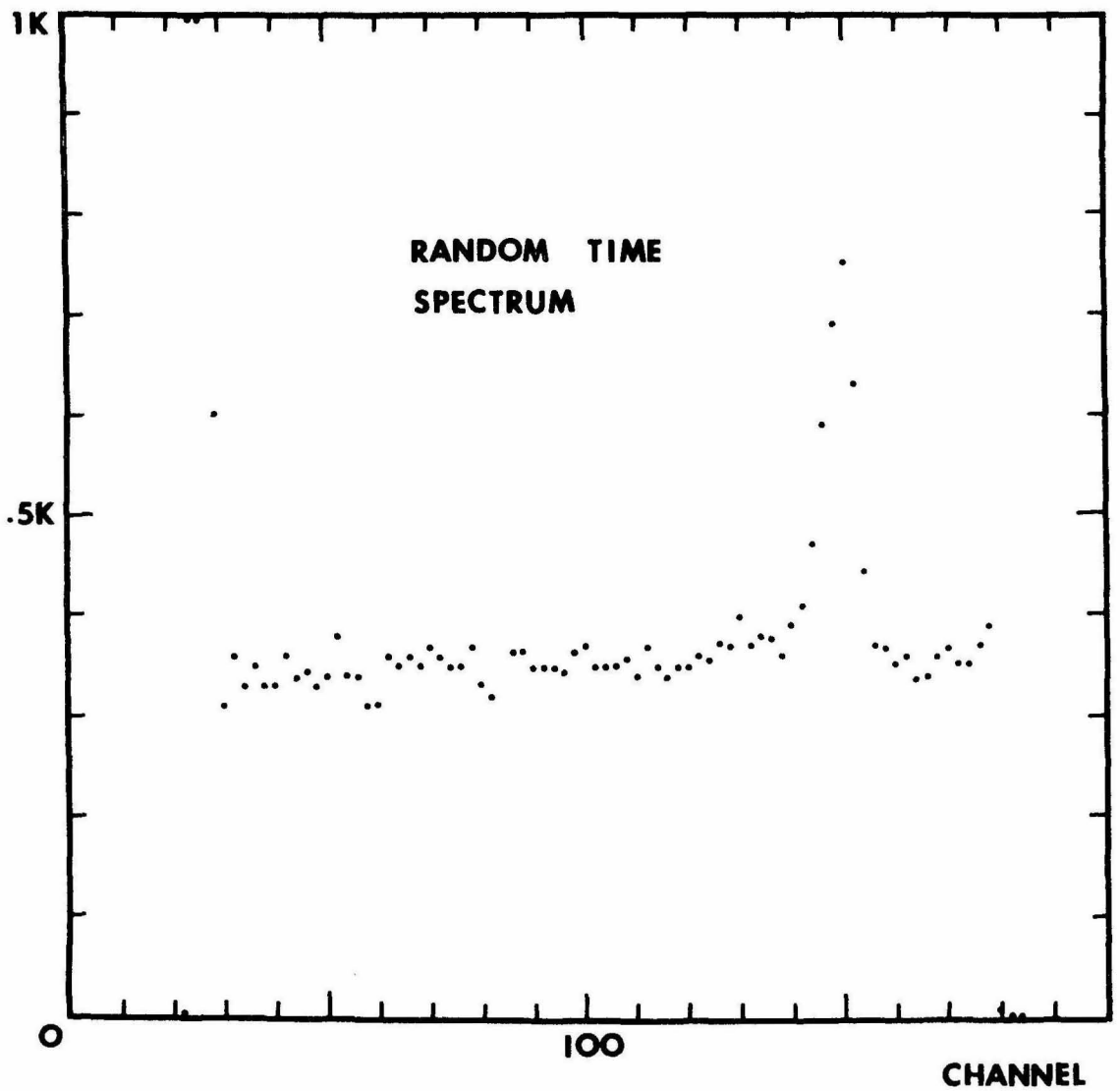

FIGURE 8

FIGURE 9

Neutron energy versus flight time calibration.

The monoenergetic neutrons were produced by the $^{14}C(p,n)^{14}N^*$ reaction. The absolute time scale is 0.641 nsec/channel. The solid curve represents a one parameter least square fit with the neutron energy E_n given by

$$E_n = m_n c^2 \left(\frac{1}{\sqrt{1 - \left(\frac{L}{\tau c \Delta C}\right)^{\theta}}} - 1 \right)$$

where m_n is the neutron rest mass, c is the velocity of light, ΔC is the channel difference between the γ-γ peak and the neutron peak and τ is the absolute time scale. θ is a free parameter and was found to be (1.934 ± 0.019).

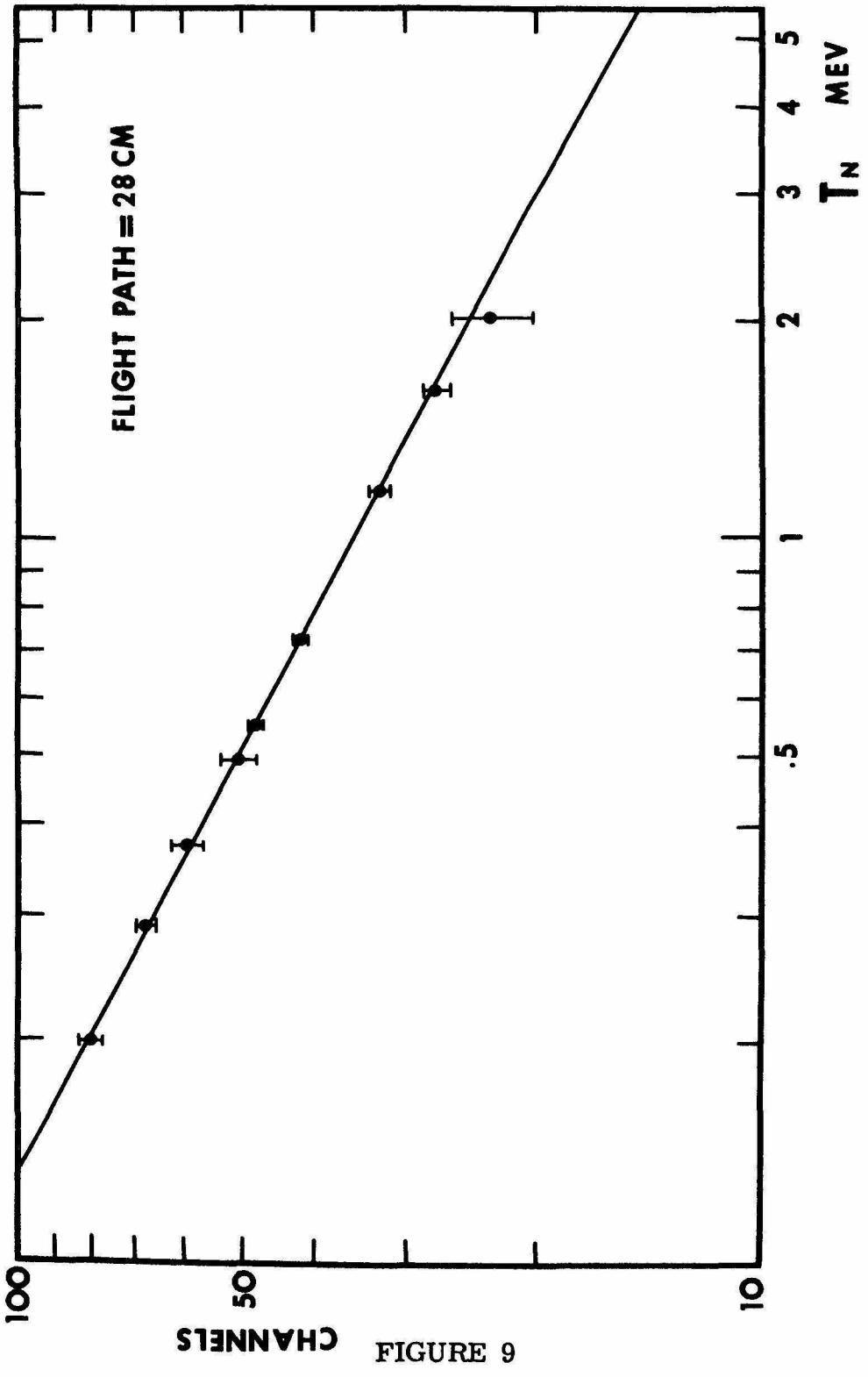

FIGURE 9

FIGURE 10

The relative efficiency of the 5" x 2" Pilot-B crystal at 80 keV neutron bias. Data points were obtained by comparing the neutron yields at 0^{o} from the $^{7}Li(p, n)^{7}Be$ reaction at various proton bombarding energies with the known cross-section. A smooth curve is drawn through the data points. The quoted error above 200 keV is ± 10% .

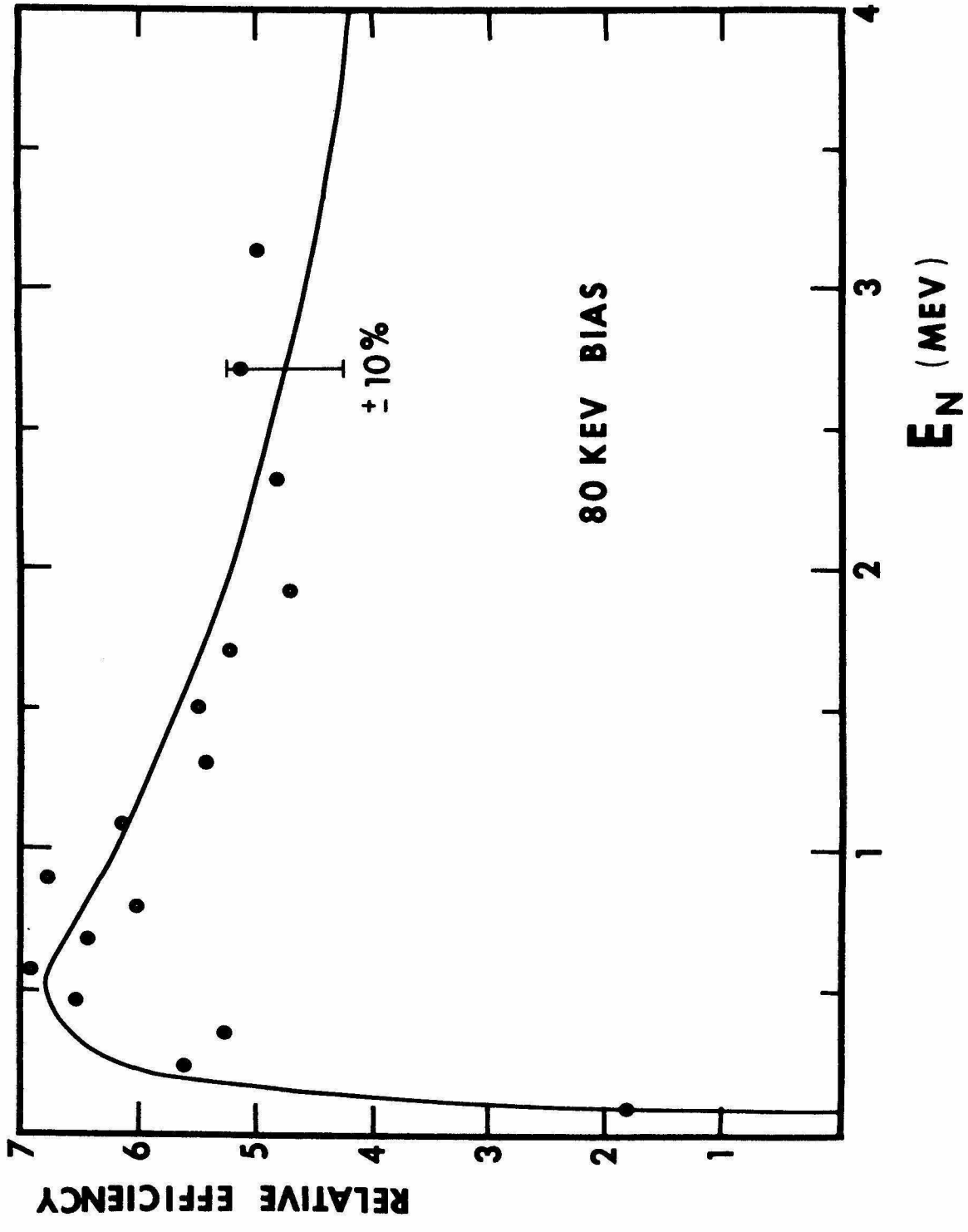

FIGURE 10

FIGURE 11

Electronic block diagram and the time sequence for each experimental cycle of the ^{9}Li half-life measurement. τ is the time base. Details are given in the text on page 18.

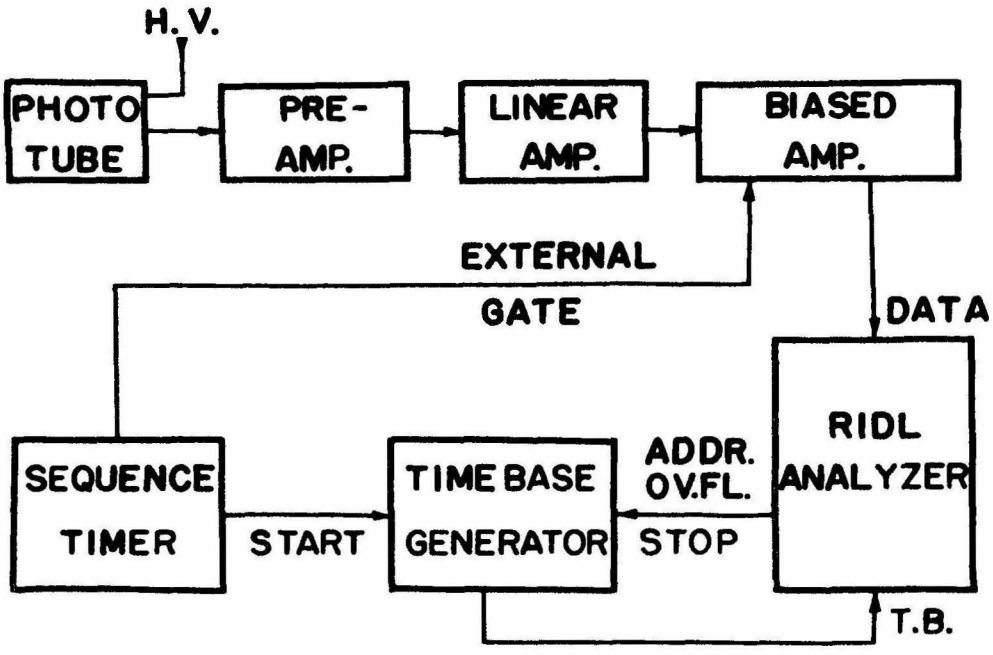
H.V.
PHOTO TUBE
PRE-AMP.
LINEAR AMP.
BIASED AMP.
EXTERNAL GATE
DATA
SEQUENCE TIMER
START
TIME BASE GENERATOR
ADDR. OV.FL.
STOP
RIDL ANALYZER
T.B.

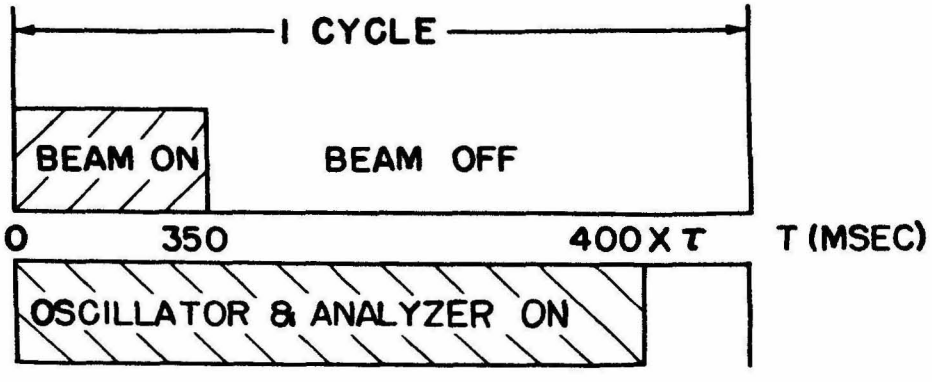
1 CYCLE
BEAM ON
BEAM OFF
0
350
400 X τ
T (MSEC)
OSCILLATOR & ANALYZER ON

FIGURE 11

FIGURE 12

The beta activities from the bombardment of the ZrT target with a 14 MeV $^{7}Li^{+++}$ beam.

The time base was 20 msec/channel. The solid curve is the sum of three decaying components. 4% of the total counts are assumed to be from ^{8}Li activity and 8% are from ^{16}N activity. The main component arises from the ^{9}Li activity. Its half-life is determined to be (177 ± 3) msec.

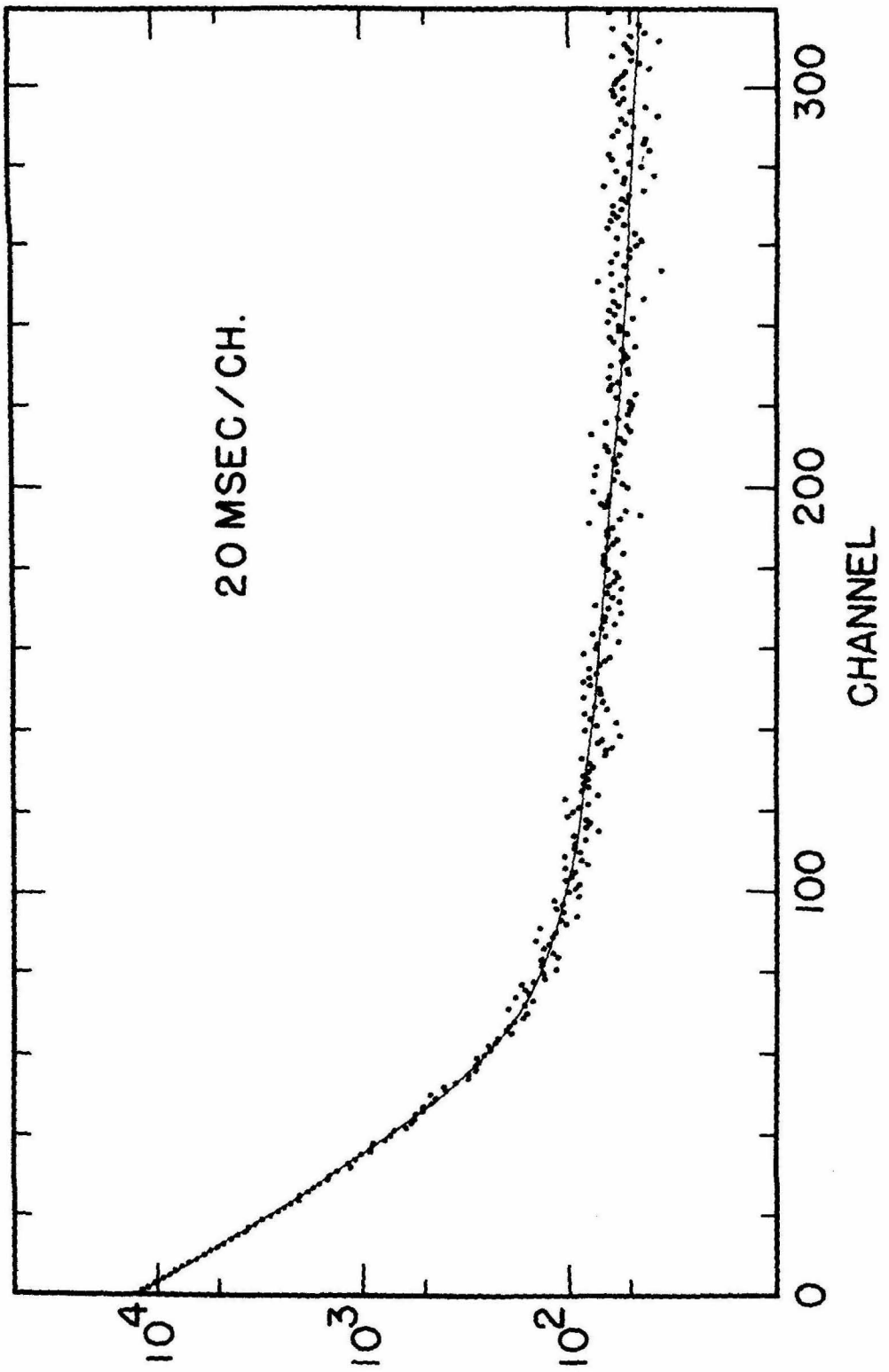

FIGURE 12

FIGURE 13

The delayed neutron time-of-flight spectrum of the first and second mean lives after the ^{9}Li decay. No correction was made for the relative efficiency of the neutron counter. The flight path is 28 cm.

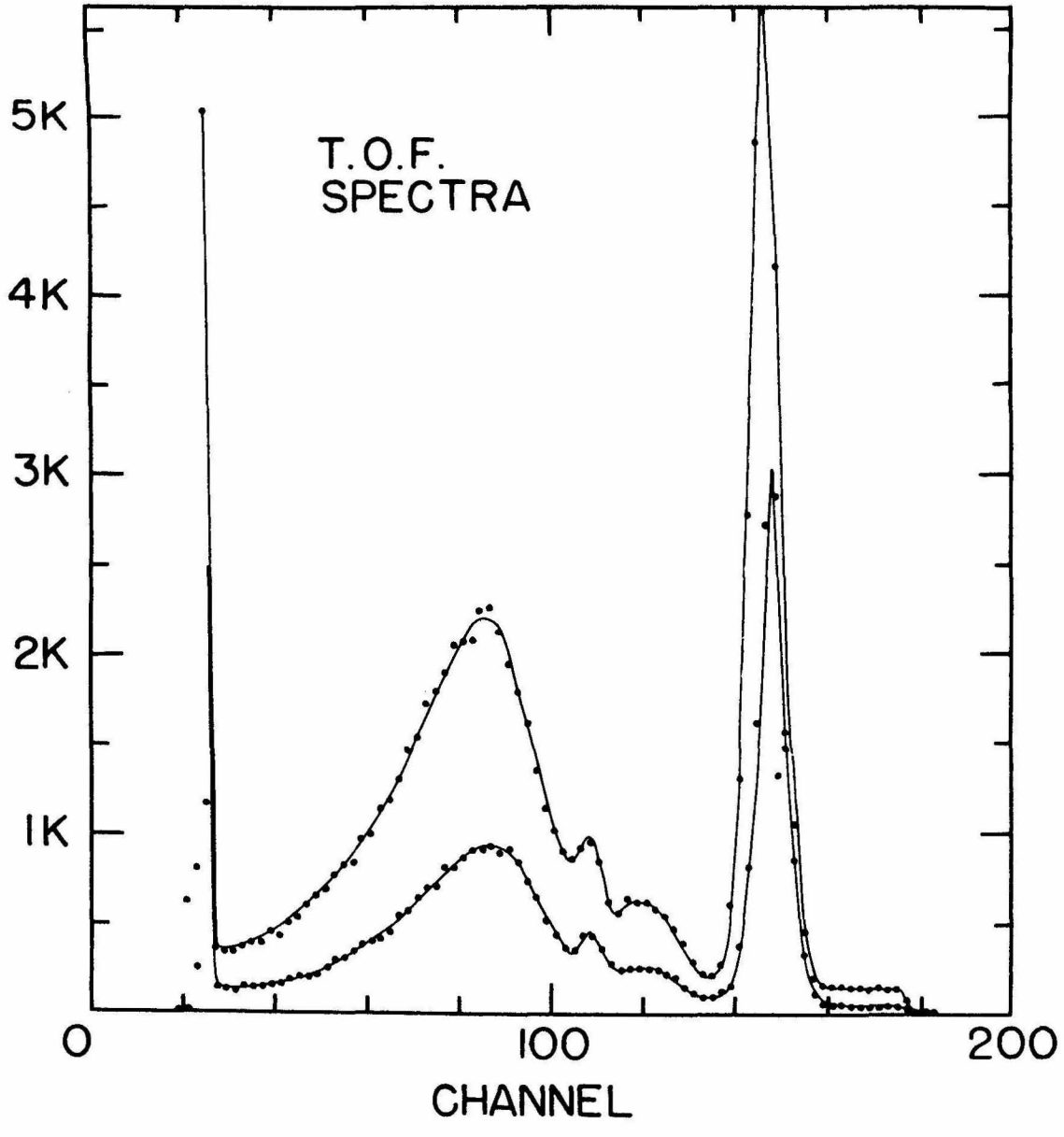

FIGURE 13

FIGURE 14

Sum of the first and second halves of the time-of-flight spectrum with the correction of the relative efficiency for the neutron counter. Peak P1 is due to the break up of the 2.43 MeV state in ^{9}Be into a neutron and two alpha particles. P2 is due to the break up of the same state through f-wave neutron emission to the ground state of ^{8}Be, which breaks up into two alphas. P3 is attributed to a new state in ^{9}Be at an excitation energy of 2.78 MeV, which breaks up almost entirely through p-wave neutron emission to the ground state of ^{8}Be.

The solid curves show the separate contributions from the three peaks (see text, page 20).

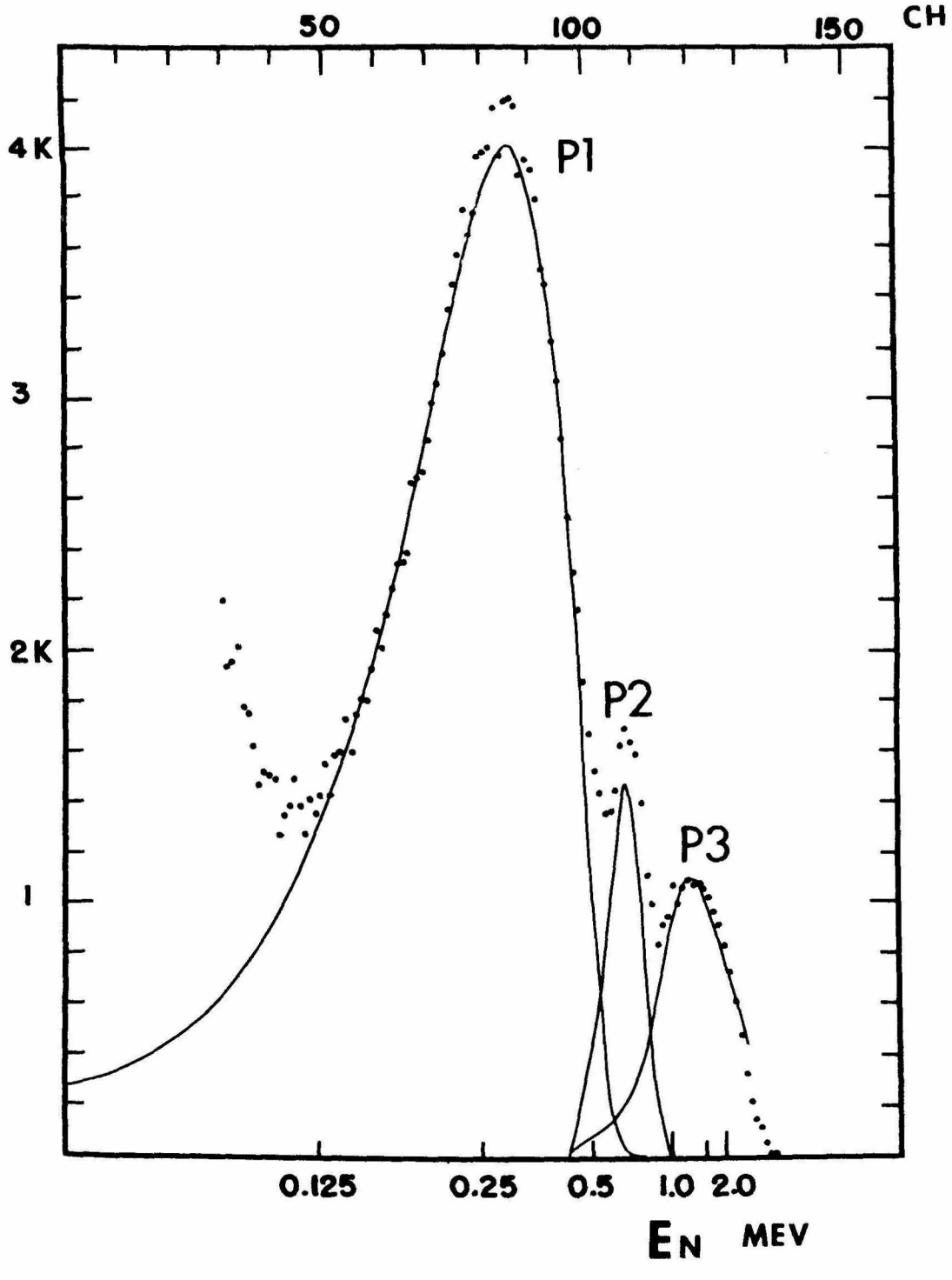

FIGURE 14

FIGURE 15

The delayed neutron energy spectrum.

The solid curve is a theoretical fit to the broad peak by assuming that the break up of the 2.43 MeV state in ^{9}Be is sequential. The broken line represents the d-wave contribution from the α-α final state interaction. The dashed line represents the s-wave contribution. Details are given in text, page 22.

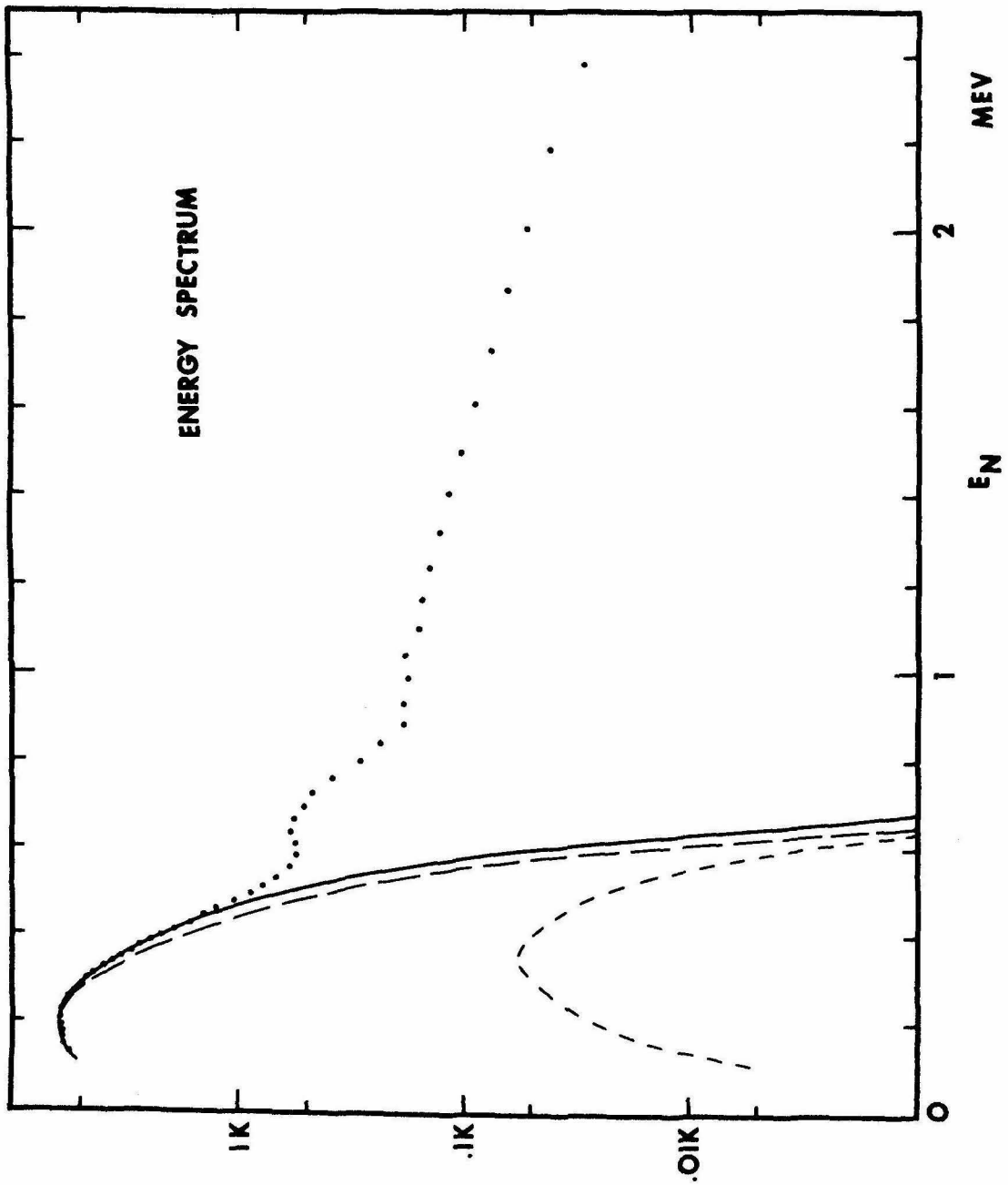

FIGURE 15

FIGURE 16

The separation of P2 and P3.

The broad peak is fitted with a single level R-matrix resonance formula. The resonance energy and the width were found to be 1.00 ± 0.1 MeV and 0.98± 0.1 MeV. Or, in terms of the excitation energy in ^{9}Be, it corresponds to a state at an excitation energy of 2.78 ± 0.125 MeV with neutron center-of-mass width of 1.1 ± 0.125 MeV (see text, page 25).

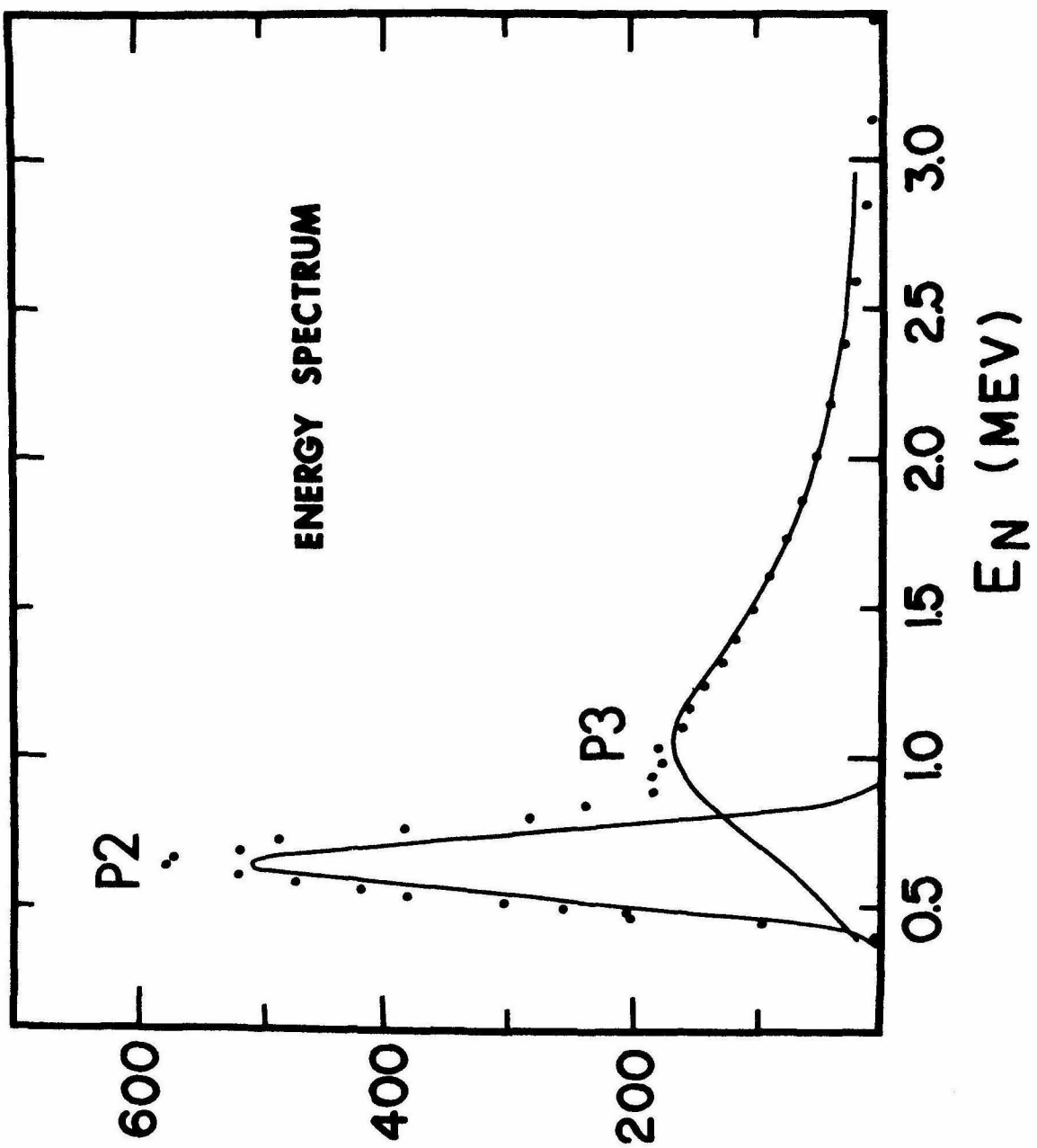

FIGURE 16

FIGURE 17

The delayed alpha spectrum of ^{9}Li from the recoil-particle method. The total number of gate pulses were 5,341.

The broken line represents a theoretical estimate of the beta contribution from the ^{9}Li decay branch to the ground state of ^{9}Be. The origins of P1, P2 and P3 are given in figure 14. The solid curve corresponds to the same theoretical calculation given in figure 15.

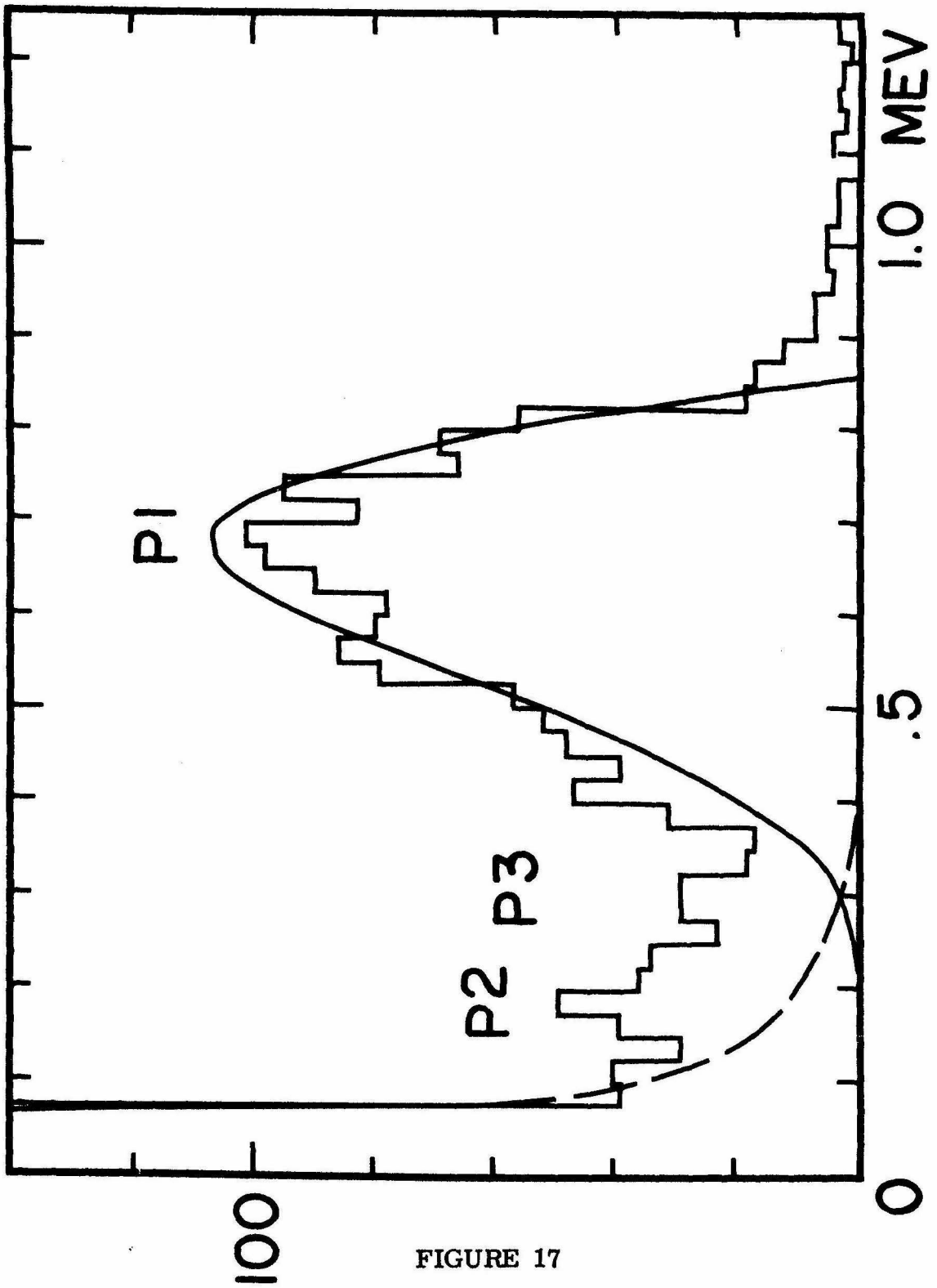

FIGURE 17

FIGURE 18

Calculated level diagram for low lying normal parity states from the rotational model.

The K = 3/2 and the K = 1/2 bands are assumed to have the same deformation. The deformation parameter δ is chosen to be 0.7. Details are given in the text, part IV, section B.

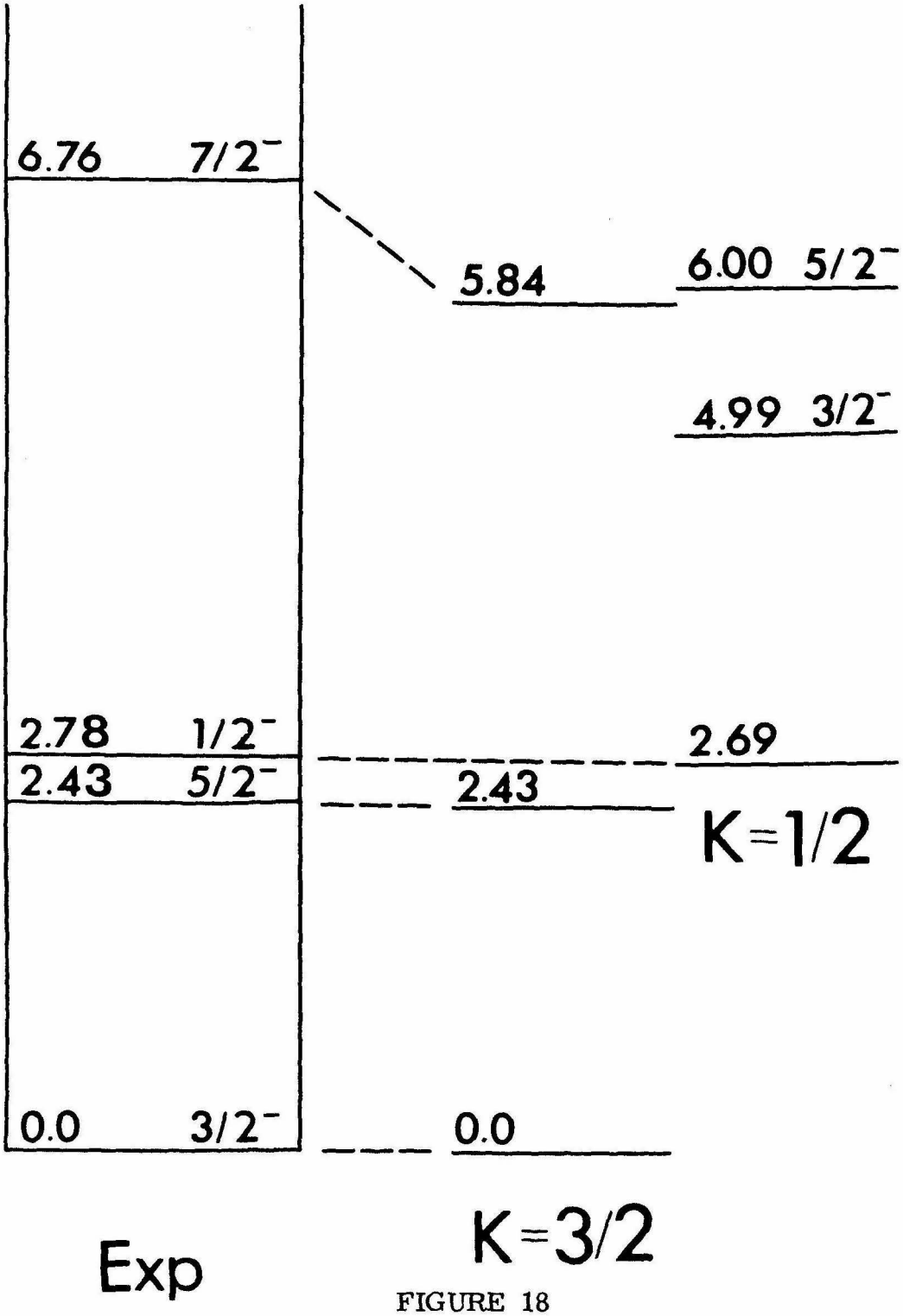

FIGURE 18